ForWind
Zentrum für Windenergieforschung
Bremen
Hannover
Oldenburg

Leibniz
Universität
Hannover

Probabilistic Safety Assessment of Offshore Wind Turbines

Annual Report 2011

7th February 2012

Cover: Windturbines on the ocean © Zentilia

Research Project:	Probabilistic Safety Assessment of Offshore Wind Turbines (PSA) Probabilistische Sicherheitsbewertung von Offshore-Windenergieanlagen (PSB)
Sponsored by:	Ministry for Science and Culture in Lower Saxony Niedersächsisches Ministerium für Wissenschaft und Kultur
Support Code:	GZZM2547
Research Period:	01.12.2009 – 30.11.2014
Reference Period:	01.12.2010 – 30.11.2011
Homepage:	www.psb.uni-hannover.de

All institutes are members of ForWind and belong to the Leibniz Universität Hannover:

Institute of Concrete Construction
Prof. Dr.-Ing. Steffen Marx / Dr.-Ing. Michael Hansen (Coordination)

Institute of Building Materials Science
Prof. Dr.-Ing. Ludger Lohaus

Franzius Institute of Hydraulics, Waterways and Coastal Engineering
Prof. Dr.-Ing. habil. Torsten Schlurmann

Institute for Geotechnical Engineering
Prof. Dr.-Ing. Martin Achmus

Institute for Steel Construction
Prof. Dr.-Ing. Peter Schaumann

Institute of Structural Analysis
Prof. Dr.-Ing. habil. Raimund Rolfes

Institute for Drive Systems and Power Electronics
Prof. Dr.-Ing. Axel Mertens / Prof. Dr.-Ing. Bernd Ponick

Institute of Electric Power Systems
Prof. Dr.-Ing. habil. Lutz Hofmann

Institute of Machine Elements, Engineering Design and Tribology
Prof. Dr.-Ing. Gerhard Poll

Insitute of Turbomachinery and Fluid Dynamics
Prof. Dr.-Ing. Jörg Seume

Content

1 Introduction 1

2 Work Packages (WP) 2

2.1 Safety of Offshore Wind Turbines (WP 1) 2

2.2 Action Effects of Wind and Waves (WP 2) 12

2.3 Soil (WP 3) 19

2.4 Foundation and Support Structure (WP 4) 26

2.5 In-Situ Assembly (WP 5) 32

2.6 Monitoring of Mechanical Components (WP 6) 35

2.7 Diagnostic Systems for Electronic Systems (WP 7) 41

2.8 Reliability of the Grid Connection (WP 8) 47

3 Summary 53

4 Literature 54

4.1 Publication List 54

4.2 Doctoral, Diploma, Master and Bachelor Theses 54

1 Introduction

Institute of Concrete Construction
Boso Schmidt, Michael Hansen

The ForWind research project Probabilistic Safety Assessment of Offshore Wind Turbines is sponsored by the Ministry for Science and Culture in Lower Saxony since 1.12.2009. In this research project safety assessments of the support structure and specific electrical and mechanical engineering components of Offshore Wind Turbines (OWT) are performed. The annual report 2010 contains first project descriptions. Annual report 2011 continues with first results of current work.

The project partners of various faculties are united by methods and input data for reliability analysis. Therefore, a central database is applied and expanded continuously through the project partners. The quality of a probabilistic analysis depends primarily on the number of measurement data and on the accuracy with which a statistical distribution function is adapted to the histogram of measurements. The reference period is increased and current data are included in the analysis. To have the opportunity to compare the results, the reference periods are matched between the project partners.

The safety assessment of the whole OWT and the considered components is divided into work packages (WP), which are summarized briefly below.

The WP 1 provides the methods and tools for probabilistic analysis. Therefore, chapter 2.1 deals with reference periods, reliability classes, partial safety factors, target reliabilities, system reliabilities and combination of actions.

In WP 2 the characteristic parameters of aerodynamic wind loads and hydrodynamic wave loads will be determined as essential input parameters of probabilistic investigations. As a common database the FINO 1 data are considered, in particular the measurements of wind speed and significant wave height.

The study performed in WP 3 should investigate if the existing partial factors for laterally loaded piles lead to the desired safety for the geotechnical limit states. Therefore, the safety and serviceability were determined by performing Monte Carlo Simulation.

WP 4 deals with the foundation and support structure of OWT's. First, a monopile structure is implemented and reliability analysis should be done. Thus, extreme events are investigated and statistical values of action effects are determined.

The WP 5 identifies risk factors regarding grouted joints during the application process. For this purpose, the influencing variables for a sensitivity analysis are used to evaluate the quality of grouted joints.

WP 6 focuses on the development and optimization of monitoring systems on mechanical components with regard to the stochastic distribution of failure probabilities. The use of condition monitoring systems together with the basic understanding of damage mechanisms allows the early detection of damages and to prevent expensive secondary damages and downtimes.

In WP7 a search coil system to detect faults in the generator is dimensioned. For several faults, analysis of the voltage induced in the search coil system is done. Effects of existing eccentricities on the fault diagnosis are investigated, too.

Within WP 8 the reliability of different grid connection topologies is examined. Thus, a reliability model for the whole grid connection is built and the equipment containing converters are analyzed.

Workshops with industrial partners will be conducted in 2012. The input data, used in the different WPs and the further working steps will be discussed. The workshops have a thematical focus on "Banks & Insurance Companies", "Construction" and "Drivetrain". The results of the workshop will be included in the annual report 2012.

2 Work Packages (WP)

2.1 Safety of Offshore Wind Turbines (WP 1)

Institute of Concrete Construction
Michael Hansen, Boso Schmidt

2.1.1 Motivation

For onshore constructions, target reliability levels established historically have been stipulated. Based on this, optimizations for the OWT shall be represented. Particularly for action effects correlations are to be considered, too. For these examinations already known formulations and combination rules are stated. A supporting structure consists of different supporting structure parts and for every part numerous failure states are possible. Thus, such system failures are also dealt with.

2.1.2 Approach

Reference period

The calculation of the probability of failure P_f and the reliability index β can react very sensitively to changes in the stochastic model, in particular in the determination of very low failure probabilities. Therefore, a conditional probability is formulated with the value β, which applies only considering a great number of basic conditions (e.g. distribution type of the base variables). Thus, a comparison is appropriate only if it refers to the same theoretical model or to the same assumptions [1]. This also applies in particular for the influence factor of time. Due to time-dependent influences and material properties, the probability of failure is also time-dependent. Provided that the probability of failure should be employed as a safety factor, it is vital to stipulate a *reference period* for that. With regard to the uncertainties concerning the statistical information, as short as possible reference periods are appropriate. If time-dependent properties have a dominant influence on the resistance side (e.g. fatigue), however, this is unfavorable.
Reference periods for characteristic values are specified with regard to the intended life of the structure or the assumed duration of the design situation. In [2] 50 years is indicated as a planning value for design working life of buildings and usual supporting structures. [3] designates further service lives for systems for the energy generation, cf. table 1.

Table 1: Service life of different structures, cf. [3]

Technical life [year]	Electricity by ...
40	Coal
25	Gas
40	Nuclear
50	Hydro
20	Wind (onshore)
?	Wind (offshore)

The reliability index β can be converted approximately with eq. (1) to other reference periods [4].

$$\Phi(\beta_n) \approx \left[\Phi(\beta_1)\right]^n \quad (1)$$

Safety-, consequences- and reliability-classes

Depending on the use of the structures different effects may have caused by failure. Therefore, safety or reliability classes (RC) are defined for risk consideration. The reliability indices β are indicated correspondingly for three reliability classes in ultimate limit state (ULS) and serviceability limit state (SLS) with table 2.

The basic principles formulated within the framework of the European construction standards are published in [2]. These values are understood as minimum requirements for general cases and are based on calibrations according to the design guidelines of different countries. In this case, logarithmic normal distributions and Weibull distributions were applied for

the description of the resistance variables and the model uncertainty, as well as normal distributions for permanent actions and extreme value distributions for variable actions.

Table 2: Reliability index β for different reliability classes (RC)

Reference period	1 year			50 years		
Reliability class	1	2	3	1	2	3
Ultimate Limit State (ULS)	4,2[2,5]	**4,7**[1,2] 4,2[3]	5,2[2,4]	3,2[2] 3,3[4]	**3,8**[1,2,4]	4,4[2] 4,3[4]
Serviceability Limit State (SLS)	2,5[5]	**3,0**[1] 2,9[2]	3,5[4]	1,0[4]	**1,5**[1,2,4]	2,0[4]

(1) [DIN1055-100(2001)] (2) [EN1990 (2010)] (3) [JCSS (2000)] (4) [JCSS (1996)]

The stipulation of the required reliability through a reliability index β is determined not only from national experience and requirements. Primarily the selected mechanical and probabilistic modeling influence the determined reliability index as well as the projected service life. Therefore, an objective of the necessary reliability index (target reliability) serves mainly as a basis for the development of consistent design regulations, but not as an explicit specification of the existing probability of failure.

Dependent on possible consequences in [2] (table B.1 and B.2) three consequences classes (CC) and reliability classes (RC) with a corresponding required reliability are stipulated. In RC1 there exist low levels, in RC3 high levels of danger and of the loss of human lives or real values.

Table 3: Recommendation for minimum values of the reliability index β

Reliability class	Minimum value of β (P_f) for the reference period of ...				
	1 year	20 years	30 years	50 years	100 years
RC3	**5,2** ($1\cdot10^{-7}$)	4,6 ($2\cdot10^{-6}$)	4,5 ($3\cdot10^{-6}$)	**4,3** ($8\cdot10^{-6}$)	**4,3** ($1\cdot10^{-5}$)
RC2	**4,7** ($1\cdot10^{-6}$)	4,0 ($3\cdot10^{-5}$)	4,0 ($4\cdot10^{-5}$)	**3,8** ($7\cdot10^{-5}$)	**3,7** ($1\cdot10^{-4}$)
RC1	**4,2** ($1\cdot10^{-5}$)	3,5 ($3\cdot10^{-4}$)	3,4 ($4\cdot10^{-4}$)	**3,3** ($5\cdot10^{-4}$)	**3,0** ($1\cdot10^{-3}$)

A conversion of the failure probabilities from the reference period of 1 year to the reference period of 50 years is possible with eq. (2).

$$
\begin{aligned}
P_{f,50} &= \Phi(-\beta_{50}) = 1-\Phi(\beta_{50}) \\
&= 1-\left[\Phi(\beta_1)\right]^{50} \\
&= 1-\left[1-\Phi(\beta_1)\right]^{50} \\
&= 1-\left(1-P_{f,1}\right)^{50} \\
&\approx 50\cdot P_{f,1}
\end{aligned}
\qquad (2)
$$

In figure 1 the dependencies are described graphically, cf. [5]. Thus, reliability indices can also be correspondingly derived for the planning periods for Wind Turbines (WT) with 20 or more years.

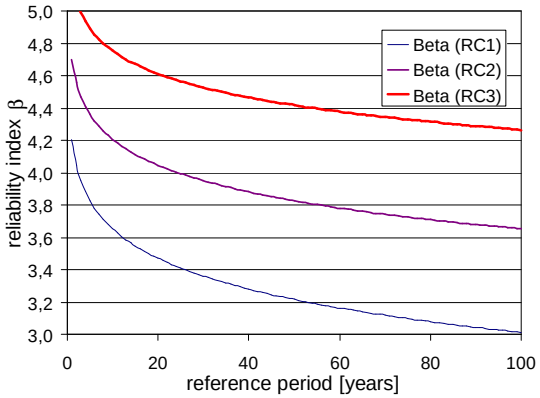

Figure 1: Dependence of the reliability index on the reference period, cf. [5]

Partial safety factors

For a practical application, a constant reliability index β is applied and constant values of the FORM sensitivity factors α_E and α_R defined in order to reduce the bandwidth of possible solutions to a single case. In [4], in case of utilization of β = 3.8 for these sensitivity factors, the fixed values α_E = –0.7 and α_R = 0.8 are applied if the condition (3) is kept.

$$0.16 < \frac{\sigma_E}{\sigma_R} < 7.6 \qquad (3)$$

Factors for actions

The characteristic values and the design values of the variable actions depend on the reference period. For the design values of the variable actions in the ULS, the reference period n = 50 years is

generally taken as a basis. These variable actions normally are Gumbel-distributed, cf. eq. (4) and [6].

$$Q_{d,50,RC2} = m_{Q,50} \cdot \left[1 - 0.7797 \cdot v_{Q,50} \cdot \left(0.5772 + \ln\left[-\ln\left(\Phi\left[(0.7 \cdot 3.8)\right]\right)\right]\right)\right] \quad (4)$$

$$Q_{d,50,RC2} = m_{Q,50} \cdot \left[1 - c(RC2) \cdot v_{Q,50}\right] = m_{Q,50} \cdot \left[1 - 3.87 \cdot v_{Q,50}\right]$$

For WT with smaller reference periods, the determining equation of the design value could be modified. Thus, the design value of the variable actions is determined with eq. (5) for a reference period of 20 years under the reliability class RC2 with β = 4.0. For the reliability class RC1 with β = 3.5 and the same reference period of 20 years, applies analogous to eq. (6). A fixed sensivity factor α_E = 0.7 is presupposed in this case.

$$Q_{d,20,RC2} = m_{Q,20} \cdot \left[1 - 0.7797 \cdot v_{Q,20} \cdot \left(0.5772 + \ln\left[-\ln\left(\Phi\left[(0.7 \cdot 4.0)\right]\right)\right]\right)\right] \quad (5)$$
$$= m_{Q,20} \cdot \left[1 - c(RC2) \cdot v_{Q,20}\right] = m_{Q,20} \cdot \left[1 + 4.20 \cdot v_{Q,20}\right]$$

$$Q_{d,20,RC1} = m_{Q,20} \cdot \left[1 - 0.7797 \cdot v_{Q,20} \cdot \left(0.5772 + \ln\left[-\ln\left(\Phi\left[(0.7 \cdot 3.5)\right]\right)\right]\right)\right] \quad (6)$$
$$= m_{Q,20} \cdot \left[1 - c(RC1) \cdot v_{Q,20}\right] = m_{Q,20} \cdot \left[1 + 3.40 \cdot v_{Q,20}\right]$$

For the three reliability classes RC1 to RC3, the dependencies of the design values of the variable actions Q_d are depicted in figure 2. The coefficient c (RC) is indicated here in the eq. (4) to (6) in each case. However, in case of the characteristic values of the variable actions, the reference period n = 50 years is applied for imposed loads (95% fractile) and n = 1 year for the environmental actions, such as e.g. wind loads (98% fractile).

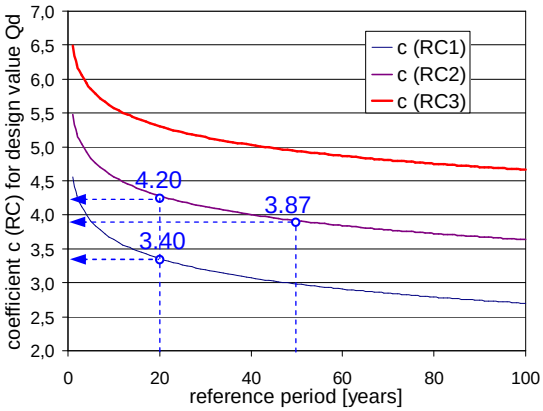

Figure 2: Dependence of the design values of the variable actions on the reliability classes and reference periods

Hence, the relationship according to eq. (7) applies for the imposed loads, on the other hand for the wind loads eq. (8) is used. For detailed information see [7], A.9.1.

$$Q_{k,il,50} = m_{Q,50} \cdot \left[1 - 0.7797 \cdot v_{Q,50} \cdot \left(0.5772 + \ln\left[-\ln\left(\Phi\left[0.95\right]\right)\right]\right)\right] = m_{Q,50} \cdot \left[1 + 1.87 \cdot v_{Q,50}\right] \quad (7)$$

$$Q_{k,wl,1} = m_{Q,1} \cdot \left[1 - 0.7797 \cdot v_{Q,1} \cdot \left(0.5772 + \ln\left[-\ln\left(\Phi\left[0.98\right]\right)\right]\right)\right] = m_{Q,1} \cdot \left[1 + 2.59 \cdot v_{Q,1}\right] \quad (8)$$

With the stipulation of a partial safety factor, the reference periods of the design values and the characteristic values must agree. The characteristic values of the climatic actions are referred with eq. (9) to the normal reference period n = 50 years.

For WT with a reference period of 20 years, the characteristic value of the wind loads can be determined with eq. (10).

$$
\begin{aligned}
Q_{k,wl,50} &= m_{Q,1} \cdot \left[1 - 0.7797 \cdot v_{Q,1} \cdot \left(0.5772 + \ln\left[-\ln\left(\Phi\left[0.98^{50}\right]\right) - \ln(50)\right]\right)\right] \\
&= m_{Q,50} \cdot \left[1 - 0.7797 \cdot v_{Q,50} \cdot \left(0.5772 + \ln\left[-\ln\left(\Phi\left[0.98^{50}\right]\right)\right]\right)\right] \\
&= m_{Q,50} \cdot \left[1 - 0.46 \cdot v_{Q,50}\right]
\end{aligned} \tag{9}
$$

$$
\begin{aligned}
Q_{k,wl,20} &= m_{Q,1} \cdot \left[1 - 0.7797 \cdot v_{Q,1} \cdot \left(0.5772 + \ln\left[-\ln\left(\Phi\left[0.98^{20}\right]\right) - \ln(20)\right]\right)\right] \\
&= m_{Q,20} \cdot \left[1 - 0.7797 \cdot v_{Q,20} \cdot \left(0.5772 + \ln\left[-\ln\left(\Phi\left[0.98^{20}\right]\right)\right]\right)\right] \\
&= m_{Q,20} \cdot \left[1 - 0.26 \cdot v_{Q,20}\right]
\end{aligned} \tag{10}
$$

The partial safety factor of the actions is calculated as a quotient from design value and characteristic value. In this way, the partial safety factor is also dependent on the reference period and the applied reliability class. In [4] the partial safety factor γ_f is stipulated for variable actions acting unfavorably, independent of the size of the coefficient of variation, such as 98% fractile with $\gamma_Q = 1.50$.

Partial safety factors deviating from this apply for OWT. Thus, the partial safety factors for ULS verifications according to table 4 are indicated in [8].

Table 4: Partial safety factors for actions γ_f according to [8]

Unfavourable loads			Favourable loads
N Normal	A Abnormal	T Transport and erection	All design situations
1.35	1.10	1.50	0.90

Similar specifications are defined in the guidelines of the Deutsches Institut für Bautechnik (DIBt) [9] and Germanischer Lloyd (GL) [10] [11], where the differences between both issues are colored and in boldface type.

Table 5: Partial safety factors γ_f of the actions for verifications in ULS [11]

Source of loading	Unfavourable loads				Favourable loads
	Type of design situation				
	N Normal	E Extrem	A Ab-normal	T Transport and erection	All design situations
Environmental	1,20	1,35	1,10	1,50	0,90
Operational	1,20	1,35	1,10	1,50	0,90
Gravity	**1,10**/1,35*	**1,10**/1,35*	1,10	1,25	**0,90**
Other initial forces	**1,20**	**1,25**	1,10	**1,30**	0,90
Heat influence	–	1,35	–	–	**0,90**

* in the event of the masses not being determined by weighing.

In [11], 4.3.7.3 is remarked that smaller safety factors may also be applied for the actions, if these have been determined through measurements or numeric analyses verified by measurements with a very high level of confidence.

Factors for resistances

The characteristic value of the yield stress f_{yk} of the reinforcing steel corresponds to the 5% fractile of the statistical distribution. For a verification, the partial safety factor is determined for the rebar according to eq. (11).

$$
\begin{aligned}
\gamma_R &= \exp\left(\left[0.8 \cdot 3.8 - \Phi^{-1}(0.05)\right] \cdot v_R\right) \\
&= \exp\left(1.395 \cdot v_R\right)
\end{aligned} \tag{11}
$$

The partial safety factor $\gamma_S = 1.15$ indicated in [12] applies correspondingly for a coefficient of variation of the yield stress of the rebar $v_s = 10\%$.

The partial safety factor for the concrete is indicated in [12] for concrete strength properties up to C50/60 with $\gamma_C = 1.50$. In the case of precast elements (PE) with a works-related and continuously monitored manufacture, this factor may be reduced to $\gamma_{C,PE} = 1.35$. The unfavorable scattering of all influence variables is registered in general by the stipulation of the coefficient of variation of $v_R \approx 0.29$ and $v_{R,PE} \approx 0.22$ (cf. [7]).

Target reliability levels

In the codes, specifications relating to the applied target reliability levels can be found only indirectly. In present semi-probabilistic verification formats, defined partial safety factors are included for stress demand and resistance variables. The product of these two safety elements leads to the global safety factor usual in former codes, which was considered exclusively on the resistance side. The partial safety factors determined by probabilistic calculations of Level II (e.g. FORM) and calibrated with methods of Level III (e.g. Monte Carlo Method, Numeric Integration) were calibrated at the existing safety level - which is not continuously constant.

The modern partial safety concept registers the uncertainties at their origin and leads in part to different results in case of consistent application in comparison to the global safety concept. This is caused e.g. through the weighting and statistical scattering of the detailed parameters for the different influences and building materials. This leads to the fact that a target reliability is uneconomical or also uncertain in some cases if it is based on the global safety concept. Therefore the stipulation of an appropriate target reliability, dependent on the construction considered and its exposure, is significant for a safety and economic design of WT.

In many countries present target reliabilities have been found by looking at the existing codes. The idea is that the application of a new approach should not lead to large differences from the existing code. The IABSE Working Commission 1 has made an inquiry into the reliability targets in a number of existing codes, cf. table 6 and [13].

Table 6: Target reliabilities β for a one year reference period as mentioned in a number of international codes, cf. [13]

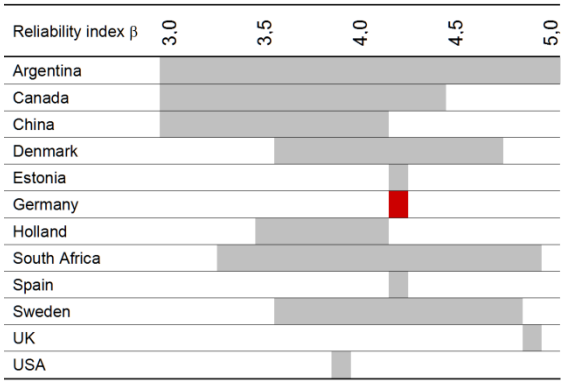

In [14], target reliability levels are formulated for WT using cost benefit analyses on a theoretical basis and [3] also specifies values for different construction parts of a WT. [15] criticizes the previous target values of the reliability levels for WT. As a result of a comparison with comparable guidelines of the oil and gas industry [16], the differences become clear, cf. table 7.

Table 7: Target reliabilities β (probability of failure P_f) for supporting structures according to [2], [17] and allocation for offshore supporting structures of the oil and gas industry [16] for a one year reference period

Relative expenses to increase safety	Failure consequences		
	Low (cf. RC1)	Medium (cf. RC2)	High (cf. RC3)
High (A)	**3,1 ($1 \cdot 10^{-3}$)** *3	3,3 ($5 \cdot 10^{-4}$) *2	3,7 ($1 \cdot 10^{-4}$) *1
Medium (B)	3,7 ($1 \cdot 10^{-4}$)	4,2 ($1 \cdot 10^{-5}$) *1	4,4 ($5 \cdot 10^{-6}$)
Low (C)	4,2 ($1 \cdot 10^{-5}$)	4,4 ($5 \cdot 10^{-6}$)	**4,7 ($1 \cdot 10^{-6}$)** *4

*1 β=4,0 ($P_f = 3 \cdot 10^{-5}$) for manned non-evacuated structures (expose level L1) [16]
*2 β=3,3 ($P_f = 5 \cdot 10^{-4}$) for manned evacuated structures (expose level L2) [16]
*3 β=3,1 ($P_f = 1 \cdot 10^{-3}$) for unmanned structures (expose level L3) [16]
*4 β=4,7 ($P_f = 1 \cdot 10^{-6}$) target reliability for structural members (RC2) acc. [2]

With reference to onshore building standards [2], [4], it seems to be clear that a smaller target reliability could be applied for unmanned OWT. Furthermore, this requirement is logic because the reliability of these OWT constructions is not in the public interest. Rather it should be defined only by the operators which suffer a

commercial loss in the case of failure. In case of a lower reliability index, higher failure probabilities are assumed. Because of the low failure consequences a classification into the reliability class RC1 would be appropriate.

System reliability

Basically two types of logical component arrangements are differentiated: the *series system* and the *parallel system.* However, in reality the logical description of the system failure corresponds rather to the model of a series system with parallel subsystems, or in the equivalent form of a parallel system with series subsystems. The status of a system is defined by the characteristics of its components. The discretization of the system into components does not necessarily correspond to the subdivision into mechanical elements, since the status of a mechanical element depends on the characteristics of its critical locations (e.g. plastic hinge). The subdivision of a system into components also depends on the form of the loading (line load, concentrated load etc.). Therefore, a mechanical element has several components and can be considered as a subsystem.

In figure 3 the theoretical interdependencies are indicated for the simple case of a series and parallel system with n = 2 limit conditions.

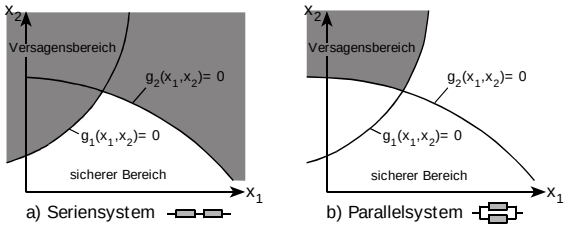

Figure 3: Failure area with parallel and series system, cf. [7]

Series systems

In a *serial system* the system failure can be expressed by the failure of one of its components ("or" link). This can be illustrated through the representation as a chain system without redundancy (figure 3a). All components equally fulfill the required function. The probability of failure of a series system corresponds to the set union of the probability of failure of its m components, cf. eq. (12).

$$P_{f,Sys(ser)} = P\left(\bigcup_{i=1}^{m}\left[g_i(x) \le 0\right]\right) = P\left(\bigcup_{i=1}^{m} F_i\right) = 1 - P\left(\bigcap_{i=1}^{m} F_i\right) \tag{12}$$

With eq. (13) trivial boundaries are indicated for rough estimates about the probability of failure of series systems. The left-hand boundary in eq. (13) indicates the exact value for uncorrelated components.

$$\max\left[P(F_i)\right] \le P_{f,Sys(ser)} \le \sum P(F_i) \tag{13}$$

This interval can be further limited with elementary bars, the so-called *Ditlevsen Bounds*, according to eq. (14) and (15).

$$P_{f,Sys(ser)}^{lower} \ge \min\begin{Bmatrix} 1 \\ P(F_1) + \sum_{i=2}^{m}\left[P(F_i) - \max_{j<i} P(F_i \cap F_j)\right] \end{Bmatrix} \tag{14}$$

$$P_{f,Sys(ser)}^{upper} \le P(F_1) + \sum_{i=2}^{m} \max\begin{Bmatrix} 0 \\ P(F_i) - P(F_i \cap F_j) \end{Bmatrix} \tag{15}$$

Parallel system

A *parallel system* first fails if all m limit states are exceeded; therefore all of its components including the strongest element fail ("and" link). Furthermore, two types of parallel systems are differentiated. The parallel systems with passive redundancy have components which are used only if other components have already failed. The parallel systems with active redundancy include components which are all effective. The failure of a component leads to the redistribution of partial functionalities over

more resilient components, however not to the system failure.

The probability of failure of a parallel system with active redundancy is described through the average quantity of the failure probabilities of its components according to eq. (16). With eq. (17), trivial boundaries can be indicated for that. The left-hand boundary indicates the exact value for uncorrelated components.

$$P_{f,Sys(par)} = P\left(\bigcap_{i=1}^{m}\left[g_i(x) \le 0\right]\right) = P\left(\bigcap_{i=1}^{m} F_i\right) \qquad (16)$$

$$\prod P(F_i) \le P_{f,Sys(par)} \le \min\left[P(F_i)\right] \qquad (17)$$

Fault, event and decision trees

Significant tools of probabilistic safety investigations and of quality management are the Fault Tree Analysis (FTA) and the Event Tree Analysis (ETA). The FTA is based on the failure of a system which is deductively attributable to the malfunction of its subsystems. This malfunctins are caused by the failure of their components. The result of these considerations is represented in the so-called fault tree, which indicates the logical links between the failure of the components and the system. In this case, only the states "Functioning / Secure" and "Failure / Insecure" are generally considered. These states are associated with probabilities of occurrence. The probability of failure of the system follows from the mathematical evaluation of the fault tree on the basis of the component malfunction, the probabilities for the occurrence of action effects and gross errors (human errors).

For a successful employment of the FTA, first of all a systems analysis is necessary. Any considered system is divided up into subsystems and components in this case. After mutual dependencies of the components have been analyzed, the investigation is restricted to the critical operating states by a limitation. In this case, the critical states must be identified within a system. The definitive "worst-case analysis" should consider the following aspects, cf. [18]:

- Stipulation of the extent of damage on a five-step scale
- Specifications about the damage duration
- Averting mechanisms

In table 8 an overview is provided of the use and the objectives of some Quality Management technologies (QM technologies). Some of these processes are also applied in current probabilistic tools [19].

Table 8: Methods and objectives of some preventive QM technologies

Methods		Objective target
FMEA	Failure Mode and Effect Analysis	Early fault detection and implementation of counteractions Systematic improvement of products and processes (risk reduction)
FTA	Fault Tree Analysis	Identification of failure sources Development and application of particular corrective actions
ETA	Event Tree Analysis	Analysis of possible sequential events
DoE	Design of Experiments	Systematic design of experiments to determine parameters of influence
Six Sigma		Product and process development for minimized nonconformity to a target value. Investigation of process quality

Further specifications relating to these processes are found for example in [18]. Analogous to the fault and event trees, decision trees for risk investigations are also dealt with in [20] and [21].

Correlation and combination of actions

Within the limit state verification, several variable actions of different origin often occur. A conservative design occurs if a load modeling is carried out over extreme value distributions in the reference period because the probability of the simultaneous occurrence of two extreme values is relatively small.

Many approaches to develop factors for this combination are based on a proposal

from *Turkstra.* According to this, several variable actions in case of simultaneous occurrence are to be combined in such a way that the dominating variable action (main action) is stipulated with its extreme value related to a specified time period. The further variable actions (accompanying actions) are applied with their respective momentary value. Every variable action is assumed once to be a main action. In this way, the number of combinations depends directly on the number of variable actions acting simultaneously. For further design, the most unfavorable value of all combinations carried out is definitive. In case of this calculation, the variable actions are assumed to be independent of each other here. However, with this regulation it is not registered that the most unfavorable situation can occur at a time which is not characterized by the maximum of one of the participating actions.

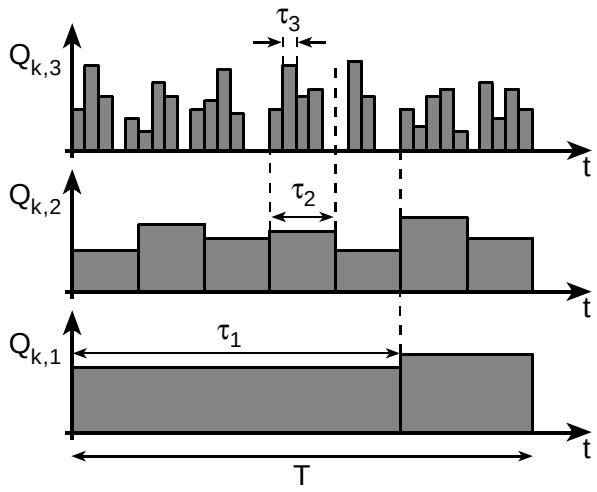

Figure 4: Loads within the reference period T (Borges-Castanheta), cf. [7]

Based on this proposal, a modified *Turkstra* regulation was proposed by the *JCSS* according to *Borges-Castanheta* (figure 4), which is also designated as a *design-value method* [21]. According to this, the reference period T of every time-variant action is first to be divided into a number of elementary time periods of similar duration τ_i, so that the extreme values of the actions in consecutive periods can be considered as independent. In addition, the conservative assumption is made that, also in case of a constantly variable action, the value of its intensity $Q_{k,i}$ is constant during the elementary time period τ_i (basic period). It is to be considered here that the shorter basic periods are integral dividers of the next larger basic periods ($\tau_i = n \cdot \tau_2 = m \cdot \tau_3$). After the period lengths have been sorted ascendingly ($\tau_3 < t_2 < \tau_1$), with the aid of the probability distributions of the actions and their extreme values $F_{i,max}(Q_{k,i})$, the necessary combinations can be carried out according to eq. (18), cf. [6], [7].

The distribution function of the extreme values $F_{Q,max}$ $(Q_{k,i})$ can be calculated from the number of load changes N_i and their distribution function F_i $(Q_{k,i})$ in the basic period τ_i with eq. (19).

$$F_{Q,\max}\left(Q_{k,i}\right) = \left[F_i\left(Q_{k,i}\right)\right]^{N_i} \tag{18}$$

$$F_{Q,\max}\left(Q_{k,i}\right) = \left(1 - P_i\left[1 - F_i\left(Q_{k,i}\right)\right]\right)^{N_i} \tag{19}$$

The factor $\psi_{0,i}$ for combined loads is calculated with eq. (20) ([6], [21]).

$$\begin{aligned}\psi_{0,i} &= \frac{F_{Q_{\max}}^{-1}\left[\Phi\left(0.4 \cdot \beta_c\right)\right]^{N_1}}{F_{Q_{\max}}^{-1}\left[\Phi\left(\beta_c\right)\right]^{N_1}} \\ &= \frac{F_{Q_{\max}}^{-1}\left(\exp\left[-N_1 \cdot \Phi\left(0.4 \cdot \beta_c\right)\right]\right)}{F_{Q_{\max}}^{-1}\left[\Phi\left(0.7 \cdot \beta\right)\right]}\end{aligned} \tag{20}$$

$$\beta_c = -\Phi\left[\frac{\Phi\left(\alpha_E \cdot \beta\right)}{N_1}\right] \qquad N_1 = \frac{T}{\tau_1} \tag{21}$$

The factor $\psi_{0,i}$ depends on the longest basic period τ_1 of the independent actions considered, the reference period T and the distribution to be applied. Some basic periods τ_1 or different loads are given with table 9. As a reference period T, the planned service life of the supporting structure is applied in general.

Table 9: Basic periods τ_1 for independent actions, cf. [6]

Load		distribution	Basic period τ_1	$N_1 = T/\tau_1$
Dead weight		Normal	50 years	1
imposed load		Gumbel	5 years	10
Snow	Continental climate	Gumbel	0,25 years	200
	Maritime climate	Gumbel	0,125 years	400
Wind		Gumbel	≈ 0,008 years	6000

For different basic periods τ_1 of the loads, the factors can be determined with eq. (20) with the application of a Gumbel distribution according to eq. (22).

$$F_{Q_{max}}^{-1}(a) = 1 - 0.7797 \cdot v_{Q,T} \cdot \left(0.5772 + \ln\left[-\ln(a)\right]\right) \quad (22)$$

2.1.3 State of work

Within the design of the OWT support structures, the current 50-year-extreme-values of wind and wave loads are conservatively combined. On the basis of the wind data and sea state data of the measuring platforms in the North Sea and the Baltic Sea, the interaction of wind and waves is stochastically analyzed, cf. [22] and [23]. As a result of these investigations, correlations should be determined location-dependent. This work is part of chapter 4 and should be based on the afore-mentioned methods.

References

[1] Spaethe, G.: Die Sicherheit tragender Baukonstruktionen. Wien, New York: Springer, 1992.

[2] DIN EN 1990: Grundlagen der Tragwerksplanung; Deutsche Fassung EN 1990:2002 + A1:2005 + A1:2005/-AC:2010. Dezember 2010.

[3] Veldkamp, D.: A Probabilistic Evaluation of Wind Turbine Fatigue Design Rules. Wind Energy 2008, 11, 655-672.

[4] DIN 1055-100: Grundlagen der Tragwerksplanung, Sicherheitskonzept, Bemessungsregeln. Deutsches Institut für Normung (Hrsg.). Berlin, Köln: Beuth, März 2001.

[5] Bericht Nr. 1149 Teil 2: Zielzuverlässigkeiten, Systemwahrscheinlichkeiten und Kombination der Einwirkungen Wind und Welle – Grundlagen. Interner Bericht, Institut für Massivbau, Leibniz Universität Hannover, Januar 2012.

[6] Grünberg, J.: Sicherheitskonzept und Einwirkungen nach DIN 1055 neu. In Avak/Goris: Stahlbetonbau aktuell - Jahrbuch 2001 für die Baupraxis. Beuth, Werner, 2001.

[7] Hansen, M.: Zur Auswirkung von Überwachungsmaßnahmen auf die Zuverlässigkeit von Betonbauteilen. PhD thesis, Universität Hannover, 2004.

[8] DIN EN 61400-3: Windenergieanlagen – Teil 1: Auslegungsanforderungen für Windenergieanlagen auf offener See, Januar 2010.

[9] Germanischer Lloyd: Guideline for the Certification of Wind Turbines, Germanischer Lloyd (GL) IV Industrial Services – Part 1, Hamburg, Germany, 2010.

[10] Germanischer Lloyd: Guideline for the Certification of Offshore Wind Turbines, Germanischer Lloyd (GL) IV Industrial Services – Part 2, Hamburg, Germany, 2005.

[11] Deutsches Institut für Bautechnik (DIBt): Schriften des DIBt, Reihe B, Heft 8: Richtlinie für Windenergieanlagen, Berlin, März 2004.

[12] DIN 1045-1: Tragwerke aus Beton, Stahlbeton und Spannbeton – Teil 1: Bemessung und Konstruktion. 2008.

[13] Vrouwenvelder, T.: Reliability based code calibration. The use of the JCSS probabilistic model code. Joint Committee on Structural Safety, Workshop on Code Calibration. http://jcss.ethz.ch, 2002.

[14] Sørensen, J. D.; Toft, H. S.: Probabilistic Design of Wind Turbines. Energies 2010, 3, 241-257; doi: 10.3390/en3020241.

[15] Seidel, M.: Critical remarks regarding requirements for design of axially loaded piles. REpower System AG. Tagung „Offshore – Wind-, Wellen- und Strömungskraftwerke“ 4./5.10.2011 TU Hamburg-Harburg.

[16] DIN EN ISO 19902: Fixed Offshore Structures. Erdöl- und Erdgasindustrie - Gegründete Stahlplattformen (ISO 19902:2007); Engl. Fassung EN ISO 19902:2007. Juli 2008.

[17] Joint Committee on Structural Safety. (JCSS): Probabilistic Model Code. Part I – Basis of design. 12th draft, November 2000.

[18] Biegert, U.: Ganzheitliche modell-basierte Sicherheitsanalyse von Prozessautomatisierungssystemen. Dissertation, Universität Stuttgart, 2003.

[19] optiSLang©: Version 3.2.1, optiSLang Documentation. DYNARDO GmbH, Weimar, Germany, July 2011.

[20] Faber, M. H.: Risk and Safety in Civil Engineering. Lecture notes on Risk and Safety in Civil Engineering. Swiss Federal Institute of Technology, 2001.

[21] Joint Committee on Structural Safety (JCSS): Background Documentation, Eurocode 1 (ENV 1991), Part 1: Basis of Design. Working Document, March 1996.

[22] Ditlevsen, O.: Stochastic model for joint wave and wind loads in offshore structures. Structural safety 24 (2002), 139-163.

[23] Bericht Nr. 1149 Teil 1: Bestimmung der Windbedingungen für Offshore-Windenergieanlagen am Standort der FINO1 Messplattform. Interner Bericht, Institut für Massivbau, Leibniz Universität Hannover, Mai 2011.

2.2 Action Effects of Wind and Waves (WP 2)

Institute of Turbomachinery and Fluid Dynamics (TFD)
Benedikt Ernst, Joerg Seume

Franzius-Institute for Hydraulic, Waterways and Coastal Engineering (FI)
Mayumi Wilms, Arndt Hildebrandt,
Torsten Schlurmann

For offshore wind turbines (OWTs), aerodynamic wind loads and hydrodynamic wave loads are essential input parameters of probabilistic investigations. Therefore, in this work package characteristic parameters of the loads and the resistance of OWTs will be determined. As a common database, the wind and wave measurements at FINO 1 are used.

2.2.1 Motivation (TFD)

Amongst others, unsteady loading of OWTs is induced by wind shear, turbulence and waves. For the design of several mechanical components of OWTs, it is necessary to consider these unsteady loadings and further aeroelastic effects on the entire structure. Examples for these effects are the coupling between the main shaft torsion and the edgewise bending of the blades and the interaction between the tower and the rotor flapwise bending. Further description of the loading of wind turbines can be found in [1, 2, 3].

2.2.2 Approach (TFD)

In this part of the work package, the failure probability of rotor blades of OWTs due to aerodynamic loads will be determined. Therefore, failures as a result of fatigue and ultimate loading will be investigated. Initially, a failure mode and effect analysis (FMEA) of an OWT will be conducted. Furthermore, the aeroelastic behaviour of OWTs will be determined by taking into account stochastic wind fields at offshore locations and given structure characteristics. Therefore, 3D turbulent, stochastic wind fields will be generated based on the FINO 1 data. The aim is to investigate the impact of both, the wind field parameters as well as the structure characteristics on the aeroelastic behaviour of OWTs and on the probability of failure. Furthermore, the sensitivity of the loads and of the natural frequencies due to variations of material and/or geometric properties will be investigated.
For the investigations, the aeroelastic model of a 5 MW OWT [4], which was developed at the National Renewable Energy Laboratory (NREL), will be used. The wind fields will be generated by the simulation software TurbSim [5] and the turbine response will be computed with the aeroelastic simulation software FAST [6].

2.2.3 State of Work (TFD)

FMEA

In this work package a failure mode and effect analysis (FMEA) of a generic OWT is prepared on the basis of published information. A FMEA is a subjective analysis method, which uses a qualitative approach to identify weak points of systems or processes in order to prevent failures and to improve the technical reliability. A FMEA is well defined and has been used successfully in many power generation systems as well as in other industries like automotive, aeronautical, and military [7].
Initially, all system elements and the system structure have to be defined. To do this in a systematic way and due to comparability reasons, this should be based on the guideline *Reference Designation System for Power Plants* (RDS-PP) [8, 9]. There, the wind turbine (WT) is subdivided into four main systems: wind turbine system [=MD], generator system [=MK], transmission of electrical energy [=MS] and internal electrical system [=B]. This part of work package 2 focuses on the wind turbine system. The structure of the wind turbine system, which

can be further subdivided into subsystems and parts, is shown in figure 1.

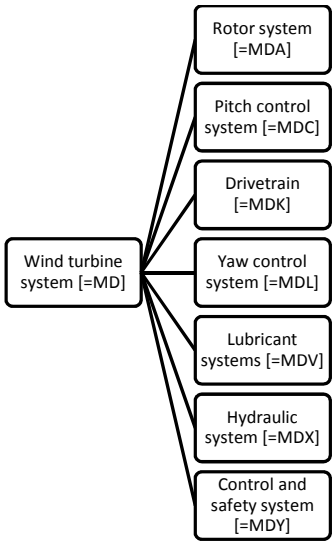

Figure 1: Structure of the wind turbine system based on RDS-PP (compare [8])

After subdivision of the selected WT, the functions and possible failure modes of each structure element have to be identified. Following this, the expected root causes must be found for each part failure mode. In [10], 16 common failure modes and 25 common root causes are identified for a typical 2 MW WT. Compared to that, 11 generic failure modes and 21 common root causes are determined in [7]. In [11], 13 top-level failure modes are found for a widespread WT of the 1.5 MW class. Furthermore, in total 33 failure modes for three functional failures are stated in [12]. In order to highlight particular areas of risk, the individual failure modes are evaluated by numerical values for the severity, occurrence and detection. The numerical scale of these three factors is typically in a range from 1 to 10. The variation of these scales depends on the applied FMEA standard and has to be defined individually. For WTs typical rating scales are given in [7, 10, 11]. Based on the severity, occurrence and detection, the risk priority number (RPN) can be calculated as follows:

RPN = Detection x Occurrence x Severity.

In order to calculate the RPNs and to indentify the high-risk systems or components, a VBA-Tool based on Microsoft Office Excel will be developed. Because of missing data of existing OWTs, critical components are derived from published FMEAs. But there are only little publications dealing with a FMEA applied to WTs or OWTs. Only a qualitative comparison of the resulting RPNs is possible, due to the subjectivity of a FMEA and differences in rating scales as well as in the analyzed WT. The analysis in [13] shows that material failure caused by corrosion, vibration fatigue and mechanical overload is the most frequently occurring failure mode for a 2 MW WT. This failure mode mainly affects the blades as well as the frame of the gearbox and the generator, all of which are critical to the WT [13]. The second most occurring failure mode is fracture, resulting from mechanical overload or shock forces. Critical components in the WT that are seriously affected by fractures are the blades and the gearbox teeth [13]. The results of [10, 11, 14] are similar to [13] and show also that the rotor system and the generator belong to the most critical components of a WT.

Effect of wind field parameters

For the design of wind turbines as well as for the calculations of the loads and the power output, the wind profile and the turbulence intensity are of special interest. In the standards IEC 61400-1 and IEC 61400-3 [15, 16], the wind profile can be described, by the so called power law profile:

$$v(z) = v_{hub}\left(\frac{z}{z_{hub}}\right)^{\alpha} \quad (1)$$

with the mean horizontal wind speed $v(z)$ at the height z above the ground (here: 40 m), the mean horizontal wind speed v_{hub} at hub height z_{hub} (here: 90 m) and the wind shear exponent α. The IEC standards [15, 16] recommend a wind shear exponent of 0.2 and 0.14,

respectively. In both IEC standards, the turbulence intensity TI is defined as the standard deviation σ_v of the horizontal wind speed related to the mean wind speed v:

$$TI = \frac{\sigma_v}{v} \quad (2)$$

The offshore turbulence intensity is described based on an approximation of the 90% percentile of the standard deviation of the horizontal wind speed [16]:

$$\sigma_{v90} = \frac{v_{hub}}{ln(z_{hub}/z_0)} + 1.28 \cdot 1.44 \cdot I_{15} \quad (3)$$

where z_0 is the surface roughness length and I_{15} is the average turbulence intensity at hub height at 15 m/s wind speed (here: 0.12). The surface roughness length z_0 has to be solved iteratively with the following equation:

$$z_0 = \frac{A_C}{g}\left[\frac{\kappa \cdot v_{hub}}{ln(z_{hub}/z_0)}\right]^2 \quad (4)$$

A_c is the Charnock parameter with $A_c = 0.011$ for open sea, κ is the von-Karman parameter with $\kappa = 0.4$ and g is the acceleration of gravity.

In order to allow a comparison taking into account site-specific wind field parameters, the wind speed measurements of the FINO 1 offshore research platform are analyzed for the period between January 2004 and December 2010. Thereby, the investigation is based on 10 min mean wind data from the FINO 1 cup anemometers. Due to wind direction fluctuations, the given standard deviation of the cup anemometers is not exactly the standard deviation of the horizontal wind speed, though close to it [17].

Figure 2 shows the comparison of the measured 90% percentile turbulence intensity and the one given in the IEC 61400-3 standard [16]. Except of wind speeds lower than 4 m/s, the measured turbulence intensities lie below the IEC-values. In figure 3, the mean values of the measured wind shear exponent is compared to the value given in the IEC 61400-3 standard [16]. At FINO 1 the measured mean wind shear exponent α is 0.09, but the results show a strong wind speed dependence. In the 18 m/s wind bin and the 19 m/s wind bin the measured wind shear exponents are slightly higher than the IEC-value.

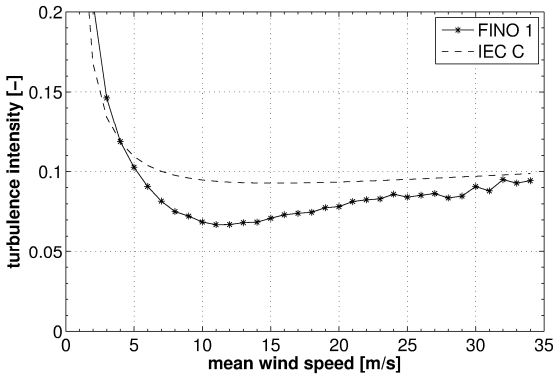

Figure 2: 90% percentile turbulence intensity depending on wind speed at 90 m height

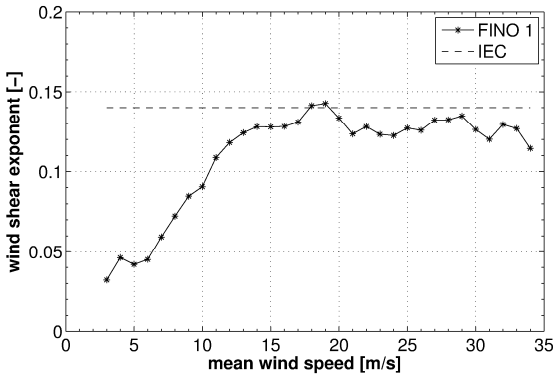

Figure 3: Mean value of the measured wind shear exponent depending on wind speed

Work in progress

Based on the comparison of the wind field parameters, aeroelastic simulations will be performed in order to investigate the effects of the loads on the OWT structure. Additionally, the effect of profile geometry variations of the aeroelastic behaviour and on the loads will be investigated.

2.2.4 Motivation (FI)

Extreme hydrodynamic loads on OWTs result from breaking waves, which cause severe impact on offshore structures and induce significant singular stresses as well as vibration and therefore discrete degradation of the support structure. The relevant loads for a design base depend on the prevalent sea state (wave height) and geometry characteristics of breaking waves (intensity of impact) in a storm. All influencing factors vary significantly in the natural sea state. For an efficient design of OWTs, dominant and significant sea state parameters as well as wave-breaking probabilities must be considered.

2.2.5 Approach (FI)

Validations with measured and computed hindcast data records are necessary and investigations on the laboratory scale are indispensable. In the first step sea state direction, heights and occurrence of wave trains in the North Sea can be analyzed. The second step deals with the wave-breaking probability, which is investigated by means of laboratory experiments in two- and three-dimensions to quantify the scatter of the influencing factors.

2.2.6 State of Work (FI)

In the first step the FINO 1 data have been analyzed on the basis of statistical analysis of extreme events to determine the design wave and design wave height according to [20]. The FINO 1 data, in particular the buoy measurements of the significant wave height determined every 30 minutes, in the time period from 01.01.2004 to 31.12.2010 have been considered. In accordance with [20] and [19] the significant wave height is determined over a time period of 3 hours. Therefore, the existing data base of FINO 1 with significant wave heights determined over 30 minutes is averaged over 3 hour time frames. For the determination of a design wave, a set of wave data has to be selected in the first place. Secondly, the data has to be properly fitted to a distribution function (e.g. Gumbel, Weibull, Gamma). Once a best-fitting distribution function is found, the design wave height is estimated by extrapolating the distribution function to the desired level of probability, which corresponds to the returning period in years, e.g. 50 years according to [20].

Data for extreme wave analysis

There are three different approaches of selecting a sample [21]:

- total sample method
- annual maxima method
- peaks-over-threshold method

The total sample method utilizes the whole data of waves heights observed during a number of years. The annual maxima method utilizes the highest significant wave height in each year. The peaks-over-threshold method takes the peak heights of waves over a certain threshold value. Because the two important requisites for a statistical sample are independency and homogeneity, the total sample method is not recommended. The annual maximal method and peaks-over-threshold method both satisfy the requisite of independency. However, the existing data base of FINO 1 sorely covers a period of 7 years. Such a short record length of extreme wave data leads to the problem of low reliability in a statistical sense. To increase the sample size, the largest significant wave height is chosen from shorter periods than a year. This method is called *n-days maxima method*. To analyze the dependency of the design wave on the data set, the following analysis focuses on the peaks-over-threshold method and the n-days maxima method. Furthermore, the sensitivity of the design wave on the selected distribution function (Gumbel, Weibull, Gamma) will be presented.

Distribution functions for extreme waves

In the extreme data analysis, many theoretical distribution functions are

employed for fitting to samples, see [21] and [22]. In this WP several distribution functions are tested. The Gumbel, Weibull and Gamma distribution function are selected because of their best-fitting parameters in the Kolmogorov-Smirnov test.
The cumulative distribution is denoted by F(x), where x stands for the extreme variate (i.e. significant wave height).

Gumbel distribution:

$$F(x) = exp\left[-exp\left(-\frac{x-\mu}{\beta}\right)\right] \quad (1)$$

with

$$\mu = m_x - \gamma\beta \quad (2)$$

$$\beta = \frac{\sqrt{6}}{\pi} * \sigma_x \quad (3)$$

Whereby m_x is the mean and σ_x the standard deviation of x, and γ the Euler constant ($\gamma = 0.577216$). μ is also called the location parameter and β the scale parameter.

Weibull distribution:

$$F(x) = 1 - exp\left[-\left(\frac{x-\mu}{\beta}\right)^k\right] \quad (4)$$

In which k is the shape parameter.

Gamma distribution:

$$F(x) = \frac{1}{\beta^k \Gamma(k)} \int_0^x t^{k-1} e^{\frac{-t}{\beta}}\, dt \quad (5)$$

Whereby Γ is the Gamma function.

For the Weibull and Gamma distribution the parameters μ, β and k are all estimated with the Maximum Likelihood method.

Return period and return value

The return period is the average time distance R (in years), in which the return value x_R is exceeded once. The parameter λ is the average rate of extreme events N_t in K years [21].

$$R = \frac{1}{\lambda[1 - F(x)]} \quad (6)$$

$$x_R = F^{-1}\left(1 - \frac{1}{\lambda R}\right) \quad (7)$$

$$\lambda = \frac{N_t}{K} \quad (8)$$

For the Gumbel distribution, the significant wave height with the recurrence period of 50 years is equivalent to the 98%-quantile value based on one year [18].

$$H_{S,50} = \mu_1 - \beta * \ln(-\ln(0.98)) \quad (9)$$

$$\mu_1 = \mu_{3h} + \beta * \ln(N) \quad (10)$$

Whereby N is the number of measured data in one year.

Design wave and design wave height

In figure 1 and figure 2 the sensitivity of the design wave $H_{S,50}$ is shown with regard to the lower threshold x_u (peaks-over-threshold method), to the n-days extreme values (n-days maxima method) and to the selected distribution function, respectively. The values range from 5.96 m to 9.28 m (peaks-over-threshold method) and from 6.98 m to 10.39 m (n-days maxima method), respectively.

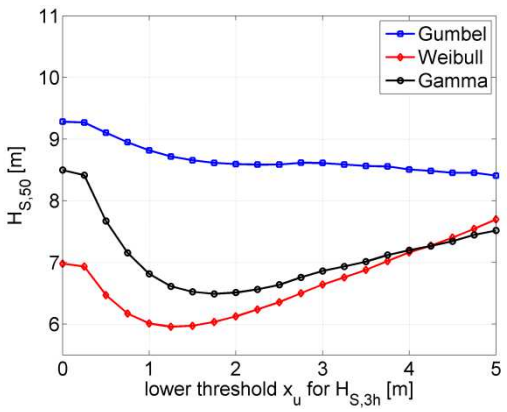

Figure 1: $H_{S,50}$ against the lower threshold x_u for the peaks-over-threshold method

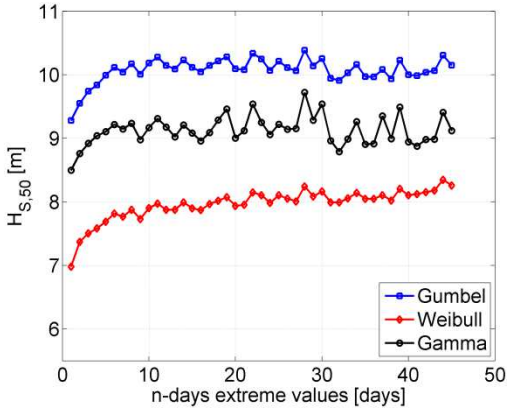

Figure 2: $H_{S,50}$ against the n-days extreme values for the n-days maxima method

In conformity with WP 4 the design wave $H_{S,50}$ is selected from the data set of 28-days extreme values and the Gumbel distribution because the minimum number of data points is met ($N_{min} \geq 50$) and the Gumbel distribution shows the best fitting with the empirical data. Thus, the design wave is $H_{S,50} = 10.38$ m. From [20] the design wave period T_D may be estimated as:

$$11.1\sqrt{H_{S,50}/g} \leq T_D \leq 14.3\sqrt{H_{S,50}/g} \quad (11)$$

$$\Longrightarrow 11.42s \leq T_D \leq 14.72s \quad (12)$$

Whereby g is the acceleration of gravity. Subsequently the design wave height H_D is estimated:

$$H_D = H_{S,50} * \sqrt{0.5 * \ln\left(T_{ref}/T_D\right)} \quad (13)$$

$$\Longrightarrow 18.87m \leq H_D \leq 19.23m \quad (14)$$

Whereby T_{ref} is the reference period (T_{ref} = 3 hrs = 10800 s). According to [20] the smaller value of the two alternative results may be used.

For time periods between 01.01.2004 and 10.02.2006 FINO 1 also provides the maximume wave height within 30 minutes intervals ($H_{max,30min}$). The maximum wave height with a returning period of 50 years is $H_{max,50} = 19.04$ m (7-days extreme values and Gumbel distribution). 7-days extreme values have to be selected to meet the minimum number of data points.

Work in progress

Due to the challenge of measuring a spatially and temporally resolved, three-dimensional wave field to analyze the probability of breaking waves, two-dimensional model tests are in progress, focusing on the optimization of the measurement system.

References

[1] Burton, T.; Sharpe, D.; Jenkins, N.; Bossanyi, E.: Wind Energy Handbook. John Wiley and Sons, 2002.

[2] Hansen, M.O.L.: Aerodynamics of Wind Turbines. 2nd Edition. Earthscan, 2008.

[3] Gasch, R.; Twele, J.: Windkraftanlagen: Grundlagen, Entwurf, Planung und Betrieb. Teubner Verlag, 2007.

[4] Jonkman, J.; Butterfield, S.; Musial, W.; Scott, G.: Definition of a 5-MW Reference Wind Turbine for Offshore System Development. National Renewable Energy Laboratory: NREL/TP-500-38060, 2009.

[5] Jonkman, B.J.: TurbSim User's B 116 D2, 1. Ausgabe, 2006.

[6] Jonkman, J.M.; Buhl Jr., M.J.: FAST User's Guide. National Renewable Energy Laboratory: NREL/TP-500-38230, 2005.

[7] Tavner, P.J.; Higgins, A.; Arabian, H.; Long, H.; Feng, Y.: Using an FMEA Method to Compare Prospective Wind Turbine Design Reliabilities. Proceedings of the European Wind Energy Conference (EWEC 2010), 20-23 April 2010, Warsaw, Poland.

[8] VGB PowerTech: Richtlinie Referenzkennzeichensystem für Kraftwerke, RDS-PP, Anwendungserläuterungen für Windkraftwerke, VGB-2009.

[9] VGB PowerTech: Richtlinie Referenzkennzeichensystem für Kraftwerke, RDS-PP, Kennbuchstaben für Kraftwerkssysteme (Systemschlüssel), VGB-B 101, 2. Auflage, 2010.

[10] Arabian-Hoseynabadi, H.; Oraee, H.; Tavner, P.J.: Failure Modes and Effects Analysis (FMEA) for Wind Turbines. Electrical Power and Energy Systems, 32 (2010) 817-824, 2010.

[11] IZP, Fraunhofer IWES, SAG, ENERTRAG: Erhöhung der Verfügbarkeit von Windkraftanlagen. Abschlussbericht, BMU Förderkennzeichen: 0327574, 2010.

[12] Andrawus, J.A.; Watson, J.; Kishk, M.; Adam, A.: Determining an Appropriate Condition-based Maintenance Strategy for Wind Turbines. The 2nd Joint International Conference on "Sustainable Energy and Environment (SEE 2006)", 21-23 November 2006, Bangkok, Thailand.

[13] Wilkinson M.; Spinato, F.; Knowles, M.: Towards the Zero Maintenance Wind Turbine. 41st Universities Power Engineering Conference, Newcastle, Sept, 2006.

[14] Fischer, K.; Besnard, F.; Bertling, L.: A Limited-Scope Reliability-Centred Maintenance Analysis of Wind Turbines. Conference Proceedings, EWEA Annual Event, 14-17 March 2011, Brussels, Belgium.

[15] International Electrotechnical Committee: IEC 61400-1: Wind turbines part 1: Design. 3rd edition, 2005.

[16] International Electrotechnical Committee: IEC 61400-3: Wind turbines part 3: Design Requirements for Offshore Wind Turbines. IEC, 1st edition, Guide: Version 1.50. National Renewable Energy Laboratory: NREL/TP-500-46198, 2009.

[17] Türk, M.; Emeis, S.: The dependence of offshore turbulence intensity on wind speed. Journal of Wind Engineering and Industrial Aerodynamics, 98 (2010) 466-471, 2010.

[18] Bergmeister, K.; Fingerloos, F.; Wörner, J.-D. (ed.): Beton-Kalender 2011 – II Windenergieanlagen in Stahlbeton- und Spannbetonbauweise. Ernst & Sohn, Berlin, Germany, 2011.

[19] DIN EN 61400-3:2009: Windenergieanlagen- Teil 3: Auslegungsanforderungen für Windenergieanlagen auf offener See. DKE im DIN und VDE, Beuth Verlag Berlin, Germany, January 2010.

[20] Germanischer Llyod: Guideline for the certification of Offshore Wind Turbines, Germanischer Lloyd Industrial Services (GL), Hamburg, Germany, June 2005.

[21] Goda, Yoshimi.: Random Seas and Design of Maritime Structures. World Scientific Publishing Co., 2000.

[22] Ochi, Michel K.: Ocean Waves. Cambridge Ocean Technology Series, 6, Cambridge University Press, 2005

2.3 Soil (WP 3)

Institute for Geotechnical Engineering
Martin Achmus, Kirill Schmoor

Offshore foundation piles can be classified into two categories according to their bearing behavior. Piles for Jacket or Tripod foundation structures are mainly axially loaded. The bearing capacity is established primarily via shaft friction. In contrast Monopiles are mainly laterally loaded and transfer the acting load via horizontal bedding into the ground. As a first step a study of a simplified Monopile model is performed as a basis for further researches.

2.3.1 Motivation

During a design process the safety for an offshore Monopile foundation structure is established by applying partial factors to the characteristic actions and soil resistances. This procedure represents the semi-probabilistic design method (Level I) according to Eurocode (EC) 0 [2] which is due to simplicity often used by practical engineers.
By applying partial factors according to EC 0 a safety index of $\beta = 3.8$ for a system with the reliability class RC2 should be established. For offshore foundation piles a corresponding safety of $\beta = 3.3$ should be realized, since Offshore Wind Turbines (OWT) can be assigned to the reliability class RC1.
By using the given partial factors in the Eurocodes for OWT the main problem to deal with is the fact that these partial factors were calibrated by applying Level II methods with certain boundary conditions and a certain safety level. In addition most of the partial factors especially for geotechnical problems are much influenced by experience which was gained in the past through different onshore constructions. So there is a need to verify these partial factors for offshore conditions with the corresponding safety level.
As a first step a simplified model of a Monopile system is investigated with a full probabilistic approach (Level III) by performing a Monte Carlo Simulation (MCS) and compared with the semi-probabilistic design method. Therefore both, the Ultimate Limit State (ULS) and the Serviceability Limit State (SLS) were considered. In addition sensitivity values for the investigated output variables were derived.

2.3.2 Approach

Introduction

First a semi-probabilistic pile design which closely fulfills the ULS and SLS proofs is obtained. For that pile design the reliability index of the foundation system and sensitivity values for the main output variables were estimated with reasonable variability of soil parameters and environmental forces by performing a MCS. Therefore typical soil and load conditions from the North Sea were assumed.

Definition of Limit States

According to the relevant German standard DIN 1054 for laterally loaded piles the ULS is defined as the ratio of the

simplicity

Level	*Basic variables*	*Reliability evaluation*	*Verification*
Level I	Deterministic variables	Partial factors (PFM), Load, resistance factors (LRFD)	Verification formula
Level II	Random variables with mean, variance and covariance	Reliability index	Target reliability index
Level III	Random variable with full distribution	Failure probability	Acceptable level of reliability Econimical optimization etc.

accuracy

Figure 1: Different levels of accuracy for uncertainty treatment

resultant horizontal force $B_{h,d}$ and the spatial ground resistance $E_{ph,d}^{spa}$ as it is shown in eq. (1):

$$\mu_{ULS} = B_{h,d}/E_{ph,d}^{spa} = \gamma_Q B_{h,k}/\frac{E_{ph,k}^{spa}}{\gamma_{R,e}} \quad (1)$$

where:

γ_Q	Partial safety factor for loading
$\gamma_{R,e}$	Partial safety factor for resistances
$B_{h,k}$	Resultant horizontal force (characteristic)
$E_{ph,k}^{spa}$	Spatial ground resistance (characteristic)

The resultant horizontal force is derived by integration of the characteristic horizontal stresses σ_h acting on the pile down to the point of rotation z_R. The spatial ground resistance is also derived down to that point. Typical distributions of the horizontal stresses are shown in figure 2.

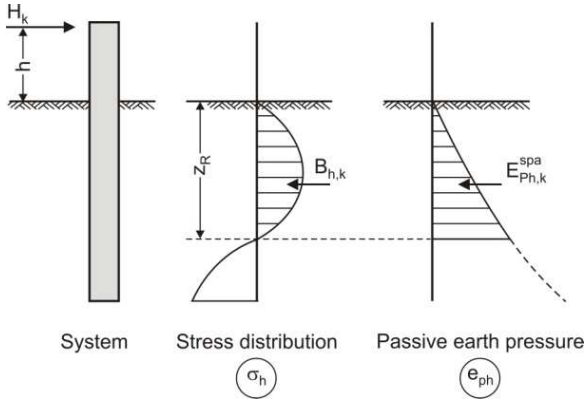

Figure 2: Elucidation of effect and resistance forces

In practical design often the limitation of the pile head displacement y_s is taken as a criterion for serviceability. For that a fixed value which often only depends on the pile diameter is chosen as a maximum allowable deflection by applying characteristic soil parameters and loading conditions. In this study serviceability is assured if the pile head displacement (at soil surface level) does not exceed the fixed value $D/40$ where D is the pile diameter:

$$\mu_{SLS} = \frac{y_s}{D/40} \quad (2)$$

where:

y_s	Pile head displacement

Calculation procedure

The calculation of the spatial ground resistance which represents the maximum achievable resistance can be done according to DIN 4085. Therefore the two-dimensional earth pressure force is multiplied by a spatial factor μ_{ph} which only depends on the ratio between the considered length from pile top down to point of rotation and the pile diameter. For a homogeneous soil layer the spatial ground resistance can be calculated according to eq. (3):

$$E_{ph}^{spa} = \frac{1}{2}\gamma' H^2 D\, K_{ph}\, \mu_{ph} \quad (3)$$

where:

H	Considered length (here $H = z_R$)
K_{ph}	Coefficient of passive earth pressure
μ_{ph}	Spatial factor

$$\mu_{ph} = \begin{cases} 1 + 0.3\,H/D & \text{for } H/D < 3.33 \\ 1.095\sqrt{H/D} & \text{for } H/D \geq 3.33 \end{cases}$$

The calculation of the pile system to obtain the pile head deflection and the actual acting stresses on the pile should be done by using the p-y method [1] which is approved for offshore pile structures.

The p-y method is a subgrade reaction method. The p-y curves implement the stiffness and strength of the ground by a non-linear relationship between the resistance of the soil and the displacement as shown in figure 3.

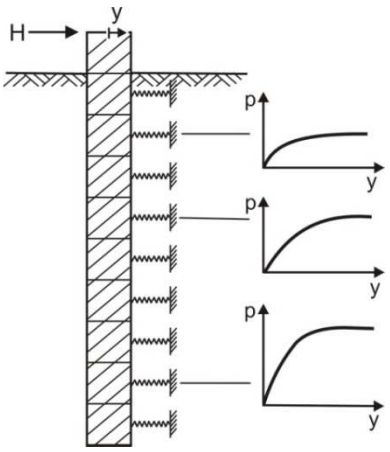

Figure 3: Implementation of soil stiffness

The main characteristics of the p-y curves are the increasing initial stiffness and maximum resistance with depth.
Each p-y curve for sand soil can be described by eq. (4) which is a function of depth z and displacement y:

$$p(y,z) = A\,p_r \tanh\left[\frac{k\,z}{A\,p_r}y\right] \qquad (4)$$

where:

z	Considered depth
y	Horizontal displacement at depth z
p_r	Controlling ultimate resistance
k	Coefficient for initial modulus of subgrade reaction
$A = (3 - 0.8\,z/D) \geq 0.9$	Correction factor

The ultimate resistance p_r for a certain depth can be derived from eq. (5) where the minimum of two failure mechanisms is obtained.

$$p_r = min\begin{cases}\gamma' z[c_1 z + c_2 D] \\ \gamma' z c_3 D\end{cases} \qquad (5)$$

where:

c_1, c_2, c_3	Dimensionless coefficients

The initial subgrade modulus k and the dimensionless coefficients c_1, c_2, c_3 from eq. (4) and (5) depend only on the internal friction angle and relative density, respectively. The relationships are shown in figure 4.

Assumed conditions

For this study typical loading conditions and ranges of soil parameters for the North Sea were assumed. Since the subsoil in the German North Sea mostly consists of dense sands with only limited intermediate cohesive layers, an idealized homogeneous dense sand profile with a typical range for the internal friction angle φ' from $36°$ to $39°$ is considered. Additionally, the corresponding range for the effective unit weight γ' was chosen from $9\,kN/m^3$ to $11\,kN/m^3$. For the horizontal force H and the pile head moment M representative values were chosen with $H = 13\,MN$ and $M = 500\,MNm$. Figure 5 shows the considered system.

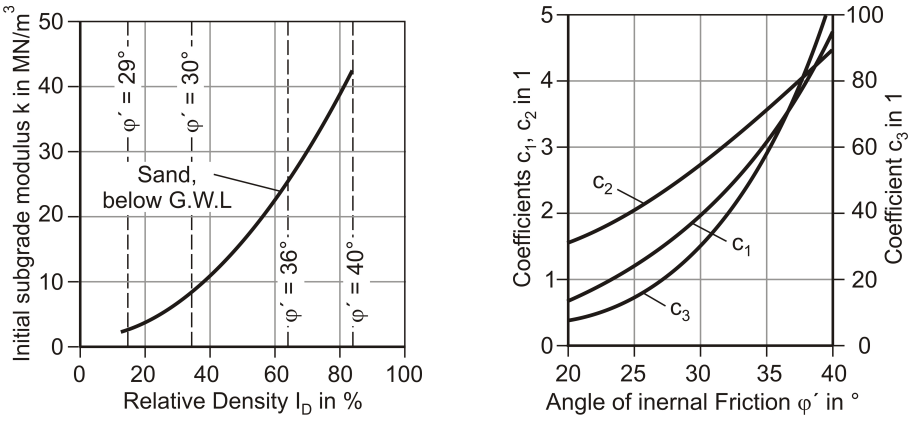

Figure 4: Coefficients for determination of p-y curves in sand soil according to API [1]

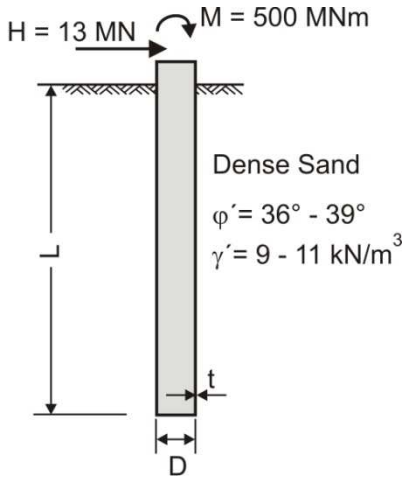

Figure 5: Considered pile system

Deterministic design

First characteristic values of the soil parameter must be chosen. In practice due to small sample size the minimum of the obtained friction angle is chosen as the characteristic value. For the effective unit weight often the mean value is assumed as the characteristic one. Based on the boundary conditions mentioned above the characteristic values are applied as $\varphi' = 36°$ and $\gamma' = 10\ kN/m^3$.

Now it is up to the designing engineer to obtain the pile length, diameter and wall thickness which maintain the mentioned limit states.

By choosing a pile length of $L = 40\ m$, a diameter of $D = 5m$ and a pile wall thickness of $t = 70\ mm$, a pile design is obtained which closely fulfills the ULS and SLS proofs. Table 1 summarizes the deterministic design procedure for the applied pile design. According to Level I method a valid pile design is found.

Probabilistic parameters

For that obtained pile design a MCS with one million realizations for each of the nine data sets was performed. Therefore the internal friction angle, the effective unit weight and the load were implemented as stochastic parameters with their typical types of distributions and Coefficients of Variation (COVs).

According to recommendations from Phoon et Kulhawy (1999) [5] [6] the COV of the friction angle was varied from $11\% - 18\%$. The COV of the unit weight was always taken into account with 10%. Because of less information the COV of the load was also varied from $15\% - 35\%$ [3]. By considering the physical bound that the moment results by multiplying the horizontal force with the moment arm, a correlation between the horizontal force and the moment of 0.7 was established. Table 2 summarizes the applied parameters which were used for the reliability analysis.

The accuracy of the estimated failure probability can approximately be computed by eq. (6) [4]:

$$COV_{pf} \approx \sqrt{\frac{1-pf_T}{pf_T\ n}} \qquad (6)$$

where:

pf_T	Target failure probability
n	Realizations performed

By assuming a target reliability index $\beta_T = 3.3$ with the corresponding failure probability of $pf_T = 4.83E\text{-}4$ and $n = 1.0E6$ realizations the COV of the estimated reliability can be specified to $COV_{pf} = 0.05$.

Table 1: Computed values for the applied pile design

Limit state	Characteristic values	Partial safety factor	Design values	Utilization ratio
ULS	$B_{h,k} = 49.2\ MN$	$\gamma_Q = 1.5$	$B_{h,d} = 73.8\ MN$	$\mu_{ULS} = 0.92$
	$E_{ph,k}^{spa} = 112.1\ MN$	$\gamma_{R,e} = 1.4$	$E_{ph,d}^{spa} = 80.1\ MN$	
SLS	$y_s = 12.21\ cm$			$\mu_{SLS} = 0.98$
	$D/40 = 12.50\ cm$			

Table 2: Stochastic parameters used for MCS

Basic variable	Notation	Mean	COV	Distribution type
Friction angle	φ′	$37.5°$	0.11 0.14 0.18	Lognormal
Unit weight	γ′	$10\ kN/m^3$	0.10	Normal
Pile diameter	D	$5\ m$	-	Deterministic
Pile length	L	$40\ m$	-	Deterministic
Pile wall thickness	t	$70\ mm$	-	Deterministic
Horizontal force	H	$13\ MN$	0.15 0.25 0.35	Gumbel
Head moment	M	$500\ MN$		

2.3.3 State of Work

Sensitivity values

First sensitivity values are calculated for the output variables like the resultant horizontal force, the spatial ground resistance and the pile head displacement. In addition sensitivity values were also computed for the ULS limit state. Sensitivity values or α-values indicate how an output variable is influenced by an input variable. α^2-values just emphasize the more important input variables in comparison to each other. Figure 6 shows the calculated results.

As can be seen, the resultant horizontal force B_h which belongs to the action side is mainly influenced by the load as it would be expected. But also the soil or resistance parameters have an influence on the resultant horizontal force, since the friction angle and the unit weight affect the

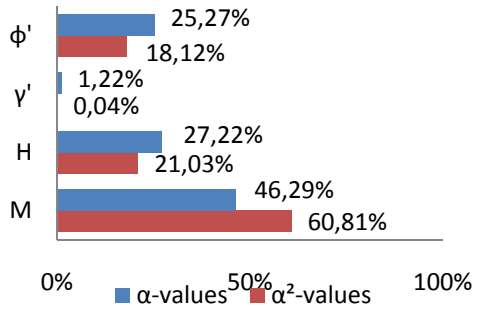

(a) Sensitivity values of B_h

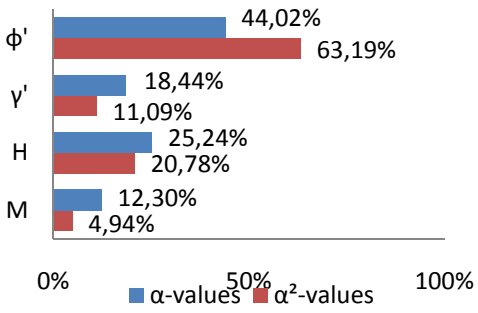

(b) Sensitivity values of E_{ph}^{spa}

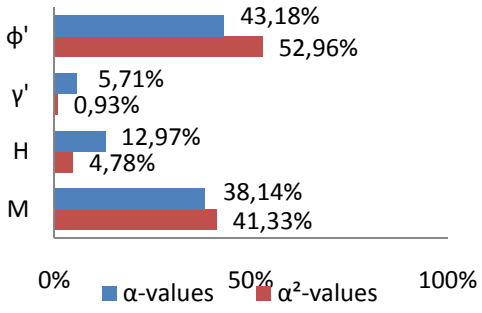

(c) Sensitivity values of y_s

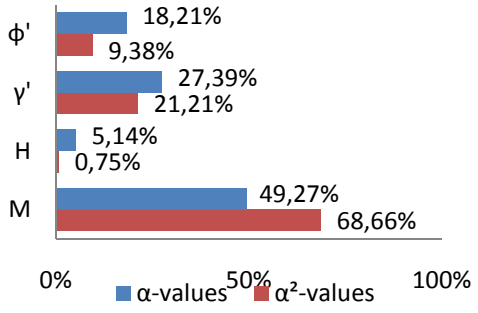

(d) Sensitivity values of the safety for ULS

Figure 6: Sensitivity values of the output variables B_h, E_{ph}^{spa} and y_s and the safety with $COV_{\varphi'} = 0.14$ and $COV_{H,M} = 0.25$

Table 3: Estimated reliability index for the deterministic pile design for ULS

	$COV_{\varphi'} = 0.11$	$COV_{\varphi'} = 0.14$	$COV_{\varphi'} = 0.18$
$COV_{H,M} = 0.15$	$\beta = \infty\ (n_{pf} = 0)$	$\beta = \infty\ (n_{pf} = 0)$	$\beta = 4.47\ (n_{pf} = 4)$
$COV_{H,M} = 0.25$	$\beta = 4.75\ (n_{pf} = 1)$	$\beta = 4.42\ (n_{pf} = 5)$	$\beta = 3.98\ (n_{pf} = 35)$
$COV_{H,M} = 0.35$	$\beta = 4.47\ (n_{pf} = 4)$	$\beta = 4.12\ (n_{pf} = 19)$	$\beta = 3.67\ (n_{pf} = 119)$

Table 4: Estimated reliability index for the deterministic pile design for SLS

	$COV_{\varphi'} = 0.11$	$COV_{\varphi'} = 0.14$	$COV_{\varphi'} = 0.18$
$COV_{H,M} = 0.15$	$\beta = 0.37$	$\beta = 0.28$	$\beta = 0.20$
$COV_{H,M} = 0.25$	$\beta = 0.34$	$\beta = 0.28$	$\beta = 0.21$
$COV_{H,M} = 0.35$	$\beta = 0.32$	$\beta = 0.28$	$\beta = 0.22$

stiffness of the ground. In the same way the spatial ground resistance is more controlled by the soil parameters, but also the load has an influence on the point of rotation and due to that also on the spatial ground resistance. The pile head deflection is almost only influenced by the internal friction angle and the moment. For the safety it can be seen that the moment is the dominant variable.

It should be mentioned that the sensitivity values are derived with reference to the mean values of the input parameters according to the proposed method by Thurner [8]. In case of the α-values for the safety it should be noticed that these values differ from the α-values derived by applying the First Order
Reliability Method (FORM) since a non-linear Limit State Function exists here.

Reliability analysis

For all calculated data sets the reliability index for the ULS and SLS are shown in table 3 and table 4. Here n_{pf} is the number of realizations in which the system failed.
As already mentioned for offshore pile foundations a suitable target reliability index for ULS would be $\beta = 3.3$. Evidently a higher reliability index even for high COV of the internal friction angle and load is established. That leads to the conclusion that in this case the design leads to very safe conditions.

For the SLS a target reliability index of $\beta = 1.5$ would be acceptable. By comparing with the computed values from table 4 it can be seen that the chosen design criterion which only depends on the pile diameter is not sufficient to be applied for deterministic SLS design. To get closer to the target reliability the embedded pile length has to be increased, so this parameter has also to be considered in the SLS proof.

Conclusions

According to the estimated reliability for ULS it can be concluded that in the case considered smaller partial safety factors could be used in the design of offshore monopile structures. For SLS a suitable criterion which also considers the embedded pile length should be chosen to achieve the target reliability. Additionally it has been shown that the pile head moment has a significant influence on the foundation safety as well as on the serviceability in comparison with the horizontal force.

The performed investigation should be seen as a first step. It is foreseen to carry out also for Tripod and Jacket foundation piles a more detailed study. The aim is to identify suitable ULS partial safety factors, which give the system reliability to be required for offshore wind tower foundations.

References

[1] API: ecommended Practice for Planning, Designing and Constructing Fixed Offshore Platforms- Working Stress Design, API (RP2A-WSD); Dallas: American Petroleum Institut, 21st edition, 2006

[2] DIN EN 1990: Eurocode: Grundlagen der Tragwerksplanung; Berlin: Deutsches Institut für Normung, 2010-12

[3] Ellingwood, B.; Galambos, T.V.: Probability based criteria for structural design; Structural Safety 1, pp. 15–26, 1982

[4] Phoon, K.-K.: Reliability-based design in geotechnical engineering; Abingdon, New York: Taylor & Francis, 2008

[5] Phoon, K. K.; Kulhawy, F. H.: Characterization of geotechnical variability, Canadian Geotechnical Journal, 36, pp. 612-624, 1999a

[6] Phoon, K. K.; Kulhawy, F. H.: Evaluation of geotechnical property variability, Canadian Geotechnical Journal, 36, pp. 625-639, 1999b

[7] Schmoor, K; Achmus, M..: On the influence of the variability of soil parameters on the behaviour of laterally loaded piles in sand, Proceeding of the 9th International Probabilistic Workshop, pp. 117-126, 2011

[8] Thurner. R.: Probabilistische Untersuchung in der Geotechnik mittels deterministischer Finite Elemente-Methode; Technische Universität Graz: Institut für Bodenmechanik und Grundbau, 2001

2.4 Foundation and Support Structure (WP 4)

Institute for Steel Construction
Peter Schaumann, Alexander Raba

Institute of Structural Analysis
Jan Goretzka, Tanja Grießmann, Raimund Rolfes

Institute of Concrete Construction
Boso Schmidt, Michael Hansen

2.4.1 Motivation

Work Package 4 (WP 4) deals with design and optimization of support structures of Offshore Wind Turbines (OWTs) with respect to probabilistic methods.
Support structures of OWTs are the load transferring link between turbine and soil. Besides dead loads of the rotor nacelle assembly (RNA) and the support structure, live loads of the RNA as well as wind and wave loads have to be transferred to the soil.
The support structure shows relatively small deviations towards design, regarding e.g. mass and load bearing capacity. Stochastic model parameters for materials such as standard deviation, type of distribution and coefficient of variance are already compiled, cf. [1].
Loads from wind and waves as well as the load bearing capacity of the soil are afflicted with great uncertainties.
Considering these uncertainties within design and optimization of support structures is possible by applying probabilistic methods and shall be investigated within WP 4.

2.4.2 Approach

For the scheduled investigations three scopes can be defined:

- Modeling,
- Loading, and
- Optimization.

Within the modeling scope a valid design basis will be defined and implemented in the finite-element software ANSYS® [2]. The implementation should be performed with greatest possible flexibility towards further investigations.
At the FINO 1 platform measured wind and sea conditions will be evaluated with regard to their extreme events for the loading scope. The Gumbel distribution, which is also used to determine other environmental conditions, represents a possible distribution to depict these extreme values, cf. figure 4. The description of input parameters with an appropriate distribution and statistical parameters allows consideration of scattering loads. The obtained load distributions shall be applied to the implemented model.
Optimization of design has to be carried out using the optimizing structural language optiSLang® [3]. Therein sensitivity analyses are to be performed to identify the important parameters of the numerical model of the investigated support structure. To achieve an adequate calculation time and lower computational costs parameters shall be reduced to a minimum. In the next step the model has to be verified by a robustness analysis. Finally reliability analyses can be performed to determine the failure probability for decisive failure modes.

2.4.3 State of Work

Modeling

For numerical simulations of a full support structure a design basis was assembled from different published reports and adjusted to project specific needs. In particular design modifications were mainly realized with respect to the site of the FINO 1 measurement platform.
The support structure can be divided into (cf. figure 1):

- RNA,
- Tower,
- Transition Piece (TP),
- Substructure, and
- Foundation.

Accordingly, the numerical model implemented in the finite-element software ANSYS® is split into separate modules for each structural part. Each module is equipped with a general interface so that it can be easily replaced.

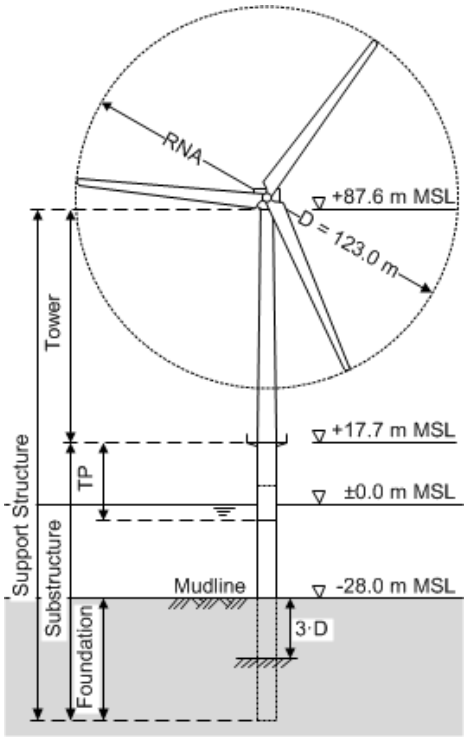

Figure 1: Offshore wind turbine with a monopile substructure.

Data for an RNA are taken from the NREL 5-MW Turbine definition [4], which is comparable to the REpower 5M and was also utilized within the OC3 Project [5]. The RNA is modeled by a single mass in the center of mass. A link between tower top and RNA mass at center of mass is realized by means of a rigid link.

The chosen tower is based on the DOWEC pre-design, which is based on a tower definition by NEG Micon Holland [6]. The DOWEC tower was also utilized within the OC3 Project [5].

The transition piece consists of a grouted joint, a tube and a platform at top of the transition piece. The platform is located at a height of +17.7 m MSL. Properties of the transition piece are similar to the monopile. Modeling a grouted joint is neglected so far.

In a first step a monopile substructure was chosen. Within the DOWEC pre-design [6] also parameters for a monopile are available.

Different from the DOWEC pre-design the water depth was modified to 28 m. For the original water depth of 20 m the wave theory is not admissible for extreme waves obtained from FINO 1 data. All relevant design parameters are presented in table 2.

The soil is simplified as a clamped bearing at three times the monopile's outer diameter below mudline. In further investigations the soil will be modeled with spring and damper elements and properties for different soil layers. For calculating the spring stiffness in dependence of the soil layer P-y-curves will be utilized. Therefore a calculation tool developed within WP 3 at the IGtH was already coupled with the ANSYS® model.

In order to validate the implemented model static equilibrium calculation and a modal analysis were conducted. Results of the modal analysis are presented in figure 2 and are compared to results of the DOWEC pre-design (cf. table 1). The slightly lower eigenfrequencies of the monopile investigated in WP 4 can be traced back to the applied modifications.

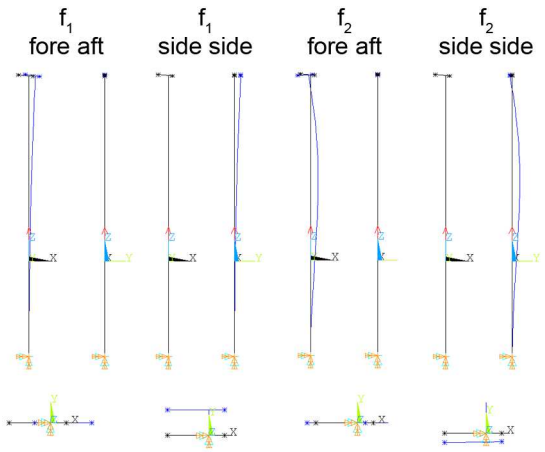

Figure 2: Eigenshapes of 1st and 2nd eigenfrequency.

Table 1: First and second eigenfrequencies of the investigated Monopile (P) compared to DOWEC (D) results [6].

	f_1 in Hz fore aft	f_1 in Hz side side	f_2 in Hz fore aft	f_2 in Hz side side
P	0.236	0.236	1.372	1.388
D	0.242	0.244	1.429	1.384
P/D	97.5 %	96.7 %	96.0 %	100.3 %

Loading

Statistical values of action effects are very important to probabilistic analysis of structural behavior. Especially for determination of extreme environmental conditions a big possible statistical population is relevant.

In order to obtain reliable statistical data and to capture seasonal fluctuations, data of FINO 1 within the 2004/01/01 – 2011/01/01 was determined.

In a first step, extreme events should be investigated, as they occur for example in load case DLC 6.1c [7]. In this context, the wind velocities at FINO 1 measurement platform were evaluated. A general description of the measuring device of the FINO 1 platform can be found in [8]. For the mentioned period values of 10-min average of wind velocities exists for eight different heights starting at 33 m up to 100 m. About 90 4-week-extreme-values were determined for each of these measuring heights.

The 10-min averages of wind velocity follows a Rayleigh distribution, cf. [7] and figure 3.

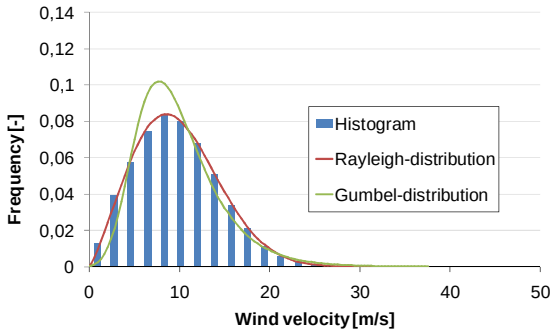

Figure 3: Histogram and different distribution functions of 10-min average values for the wind velocity in 100 m above sea level

The distribution of extreme wind velocities is more consistent with a Gumbel distribution, cf. figure 4. In addition to a visual assessment of goodness of fit, this result is confirmed by the Chi-squared-test and the Kolmogorov-Smirnov-test.

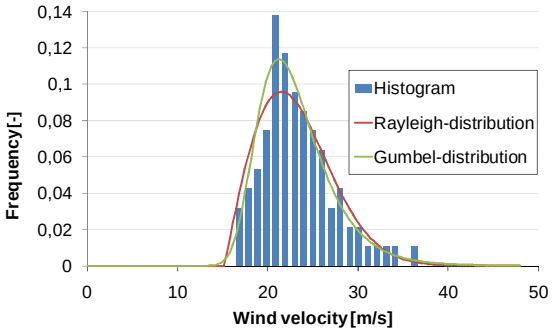

Figure 4: Histogram and different distribution functions of 4-week-extreme-values for the wind velocity in 100 m above sea level

Parameters of the statistical distribution of 4-week-extreme-values were determined for each of the eight measurement heights.

Due to the large measurement period and the height resolution an analysis of the extreme wind profile is possible. The GL [7] defines the reference wind velocity as an extreme wind velocity at hub height with a return period of 50 years. This wind velocity is equivalent to the 98%-fractile for a period of one year, cf. eq. (1).

$$1 - \frac{1}{50\ years} = 0{,}98 \qquad (1)$$

The distribution function $F_u(x)$ is determined for a Gumbel distribution (extreme value distribution Typ 1 for maximum values) by eq. (2).

$$F_u(x) = exp\{-exp[-a \cdot (x-u)]\} \qquad (2)$$

The parameters of the distribution are:

$$a = \frac{\pi}{\sqrt{6} \cdot \sigma_{Ext}} \qquad (3)$$

$$u = m - \frac{0{,}577216}{a} \tag{4}$$

For the chosen distribution, the shape of the distribution function is independent of the reference period. Thus, the standard deviation remains constant. A modified reference period leads to a parallel shift of the distribution function. Per year N = 13 4-week-extreme-values are available.

$$\begin{aligned} F_{Extr,N}(x_N) &= \left[F_{Extr,1}(x_{4-week})\right]^N \\ &= exp\,\{-exp\,[-a \cdot \\ &\quad (x_{4-weeks} - u_{4-weeks}) + ln(N)]\} \\ &= exp\{-exp[- \cdot (x_N - u_N)]\} \end{aligned} \tag{5}$$

$$\begin{aligned} u_N &= u_{4-weeks} + \frac{ln(N)}{a} \\ &= u_{4-weeks} + ln(N)\frac{\sqrt{6}}{\pi} \cdot \sigma \end{aligned} \tag{6}$$

$$m_N = m_{4-weeks} + \frac{ln(N)}{a} \tag{7}$$

The 98%-fractile for a period of one year corresponds to the characteristic value for a return period of 50 years. Alternatively, the determination of fractiles can be performed by using linear regression analysis. The results of both procedures agree very well [9].
The profile of wind velocity with a return period of 50 years is depicted in figure 5. Comparison of the measured wind profile with the approach of [7] shows an underestimation of wind velocities for the FINO 1 measurement platform. For the reference velocity at hub height (in this case 100 m) the determined reference velocity is used.

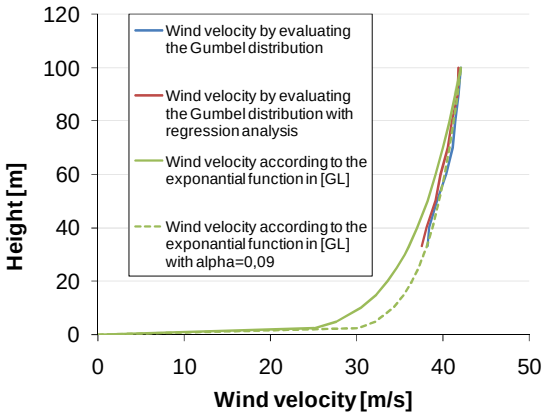

Figure 5: Profile of the 50-years-wind-velocities from measurements compared to the approach of Germanischer Lloyd [7]

Figure 5 shows an example of the exponential function according to [7] with a lower exponent. This approach better represents the analyzed wind velocities for 33 to 100 m height. Whether this nearly vertical run of the curve represents the wind velocities above 100 m respectively below 33 m cannot be verified with the available data. Further investigations of wind conditions at the site of FINO 1 are listed in WP 2 and [9].
According to the evaluation of wind velocities, extreme wave heights at the site of FINO 1 measurement platform were investigated, too. For the observation period mentioned above, respectively for the period early 2004 until mid-February 2006, 30-min values of significant wave heights and 30-min values of extreme wave heights are available.
The analysis of wave data has shown that even 1-week-extreme-values of wave heights can be described by a Gumbel distribution. 1-week-extreme-values were chosen to ensure a sufficient number of extreme values. According to previously mentioned extrapolation of extreme values, the characteristic wave height with a return period of 50 years can be determined to 19.01 m (evaluating the Gumbel distribution), respectively 19.30 m (evaluating the Gumbel distribution with regression analysis).

Optimization

During the last year knowledge in the field of probabilistic methods has been extended. In November 2011 the project partners participated in the 9th International Probabilistic Workshop in Brunswick. Furthermore, probabilistic studies on the model of the monopile have been initiated.

Sensitivity analyses for the numerical model of the chosen support structure and the statistical input parameters were performed. For this purpose the optimizing structural language optiSLang®, which can be coupled with the finite-element software ANSYS®, is accessible. The sensitivity analysis includes statements about the sensitivity of results of a modeling problem, depending on particular parameters of the probabilistic model. Mathematically, the sensitivity of an output variable y_i against changes in the input x_j can be characterized by the derivative $\partial y_i / \partial x_j$. In order to obtain meaningful correlations between the input and output variables of the model, it is important to capture the input correlations in the simulated values quite accurately (cf. [3], chap. 4).

Within sensitivity analysis, the relevant parameters are identified and adjusted appropriately. Thus, both an improvement of the model and a better understanding of the problem in terms of robustness, reliability and optimization will be possible: In this way variations of important responses within the design space can be estimated, objectives and the convergence of the model examined, and possible instabilities can be detected. Furthermore sensitivity analysis allows a dimensionality reduction of the parameter space where the optimization is made (cf. [10], chap. 1.5).

At first, a set of samples is to be generated to perform sensitivity analysis. Then the influence each input parameter has on the responses is examined. The recommended number of samples (generated with latin hypercube sampling) amounts to $N \geq 2(n_i + n_o)$, where N denotes the number of samples, n_i the number of input parameters and n_o the number of output parameters [3].

In order to estimate the parameter sensitivities multivariate statistic is used: The linear correlation coefficient indicates possible sensitivity and is regarded as an indicator to detect significant parameters.

After the sensitivity analysis has been completed, a robustness analysis verifies the model parameters. The final step within this probabilistic design focuses on a reliability analysis and optimization of the model. Therefore different methods of reliability analysis such as FORM, SORM, RSM, etc. are used (cf. [1], chap. 2.1.2). The aim is to determine the most likely failure modes of the structure.

2.4.4 Summary and Outlook

A design basis for an OWT founded on a monopile was assembled and implemented in the finite-element software ANSYS®. The finite-element model was validated by simple calculations and integrated into an experimental design (DoE) implemented in optiSLang® in order to determine appropriate sample sets.

Extreme value distributions for wind velocities and wave heights were determined at the site of the FINO 1 measurement platform. Using different methods to determine fractiles, characteristic values could be calculated with reference to common standards.

In a next step scattering load effects on OWTs will be determined from the measured distributions of wind and wave characteristics. The results will be applied to the existing model of the monopile and integrated into an enhanced sensitivity analysis in optiSLang®.

Distributions and statistical parameters of loading and resistance as well as the applied boundary conditions should be agreed in a design-workshop with industry representatives in late May 2012.

Table 2: Design parameters of the OWT with monopile. (previous values in brackets)

RNA	Rating	5 MW
	Rotor Orientation, Configuration	Upwind, 3 Blades
	Rotor, Hub Diameter	126 m, 3 m
	Hub Height	+90 m MSL
	Rotor Mass, Nacelle Mass	110 t, 240 t
Tower	Height	69.9 m (80.0 m)
	Base: Outer Diameter, Thickness	6.0 m, 0.027 m
	Top: Outer Diameter, Thickness	3.87 m, 0.019 m
	Density	8500 kg/m³
	Mass	219 t (250 t)
TP	Base Height	-4.5 m MSL (-10.0 m MSL)
	Top Height	+17.7 m MSL (+10.0 m MSL)
	Outer Diameter, Thickness	6.0 m, 0.060 m
	Mass	211 t (190 t)
Monopile	Base Height	-46.0 m MSL (-20.0 m MSL)
	Top Height	-4.5 m MSL (-10.0 m MSL)
	Outer Diameter, Thickness	6.0 m, 0.060 m
	Mass	395 t

References

[1] Probabilistic Safety Assessment of Offshore Wind Turbines, annual report 2010, Leibniz Universität Hannover, February 2011.

[2] ANSYS®: Release 13.0, Documentation ANSYS, SAS IP, Inc ed., USA, 2010.

[3] optiSLang®: Version 3.2.1, optiSLang Documentation, DYNARDO GmbH, Weimar, Germany, July 2011.

[4] Jonkman, J.; Butterfield, S.; Musial, W. and Scott, G.: Definition of a 5-MW Reference Wind Turbine for Offshore System Development. NREL/TP-500-38060. NREL: Golden, CO, 2009.

[5] Jonkman, J.; Musial, W.: IEA Wind Task 23 Offshore Wind Technology and Deployment – Subtask 2 The Offshore Code Comparison Collaboration (OC3) – Final Report. NREL: Golden, CO, 2010.

[6] Kooijman, H.J.T.; Lindenburg, C.; Winkelaar, D. and van der Hooft, E.L.: DOWEC 6 MW Pre-Design: Aero-elastic modeling of the DOWEC 6 MW pre-design in PHATAS. DOWEC-F1W2-HJK-01-046/9 public version. ECN: Petten, 2003.

[7] Germanischer Llyod: Guideline for the certification of Offshore Wind Turbines, Germanischer Lloyd Industrial Services (GL), Hamburg, Germany, June 2005.

[8] Neumann, T.; Herklotz, K.: Erste Betriebserfahrungen mit der FINO1-Forschungsplattform in der Nordsee, DEWI Magazin Nr. 24, Germany, February 2004

[9] Bericht Nr. 1149 Teil 1: Bestimmung der Windbedingungen für Offshore-Windenergieanlagen am Standort der FINO1 Messplattform. Interner Bericht, Institut für Massivbau, Leibniz Universität Hannover, Mai 2011.

[10] Saltelli, A.; Chan, K.; Scott, E.M.: Sensitivity Analysis. John Wiley & Sons, Ltd, Chichester, England, 2000.

2.5 In-Situ Assembly (WP 5)

Institute of Building Materials Science
Ludger Lohaus, Michael Werner

2.5.1 Motivation

Support structures and turbines of offshore wind turbines (OWTs) itself are segmental prefabricated onshore which offers the possibility to monitor the production and to ensure the quality. By contrast, the foundation and the connection elements between the support structure and the foundation are manufactured offshore. Frequently a so-called grouted-joint is used. The gap between the pile and the sleeve is filled with a high performance mortar called “grout”. These grouted joint connections are used in almost all kinds of offshore structures.
The main problem during the installation process is the application of the grout under offshore conditions [1]. Due to the inaccessibility of the application site, it is difficult to establish an effective quality control and quality management system that induces a high safety factor in the design of the grouted joint connection.

2.5.2 Approach

In this work package “supporting structure production in situ”, the risk factors of the grouted joints during the application process will be evaluated taking into account the material behaviour of the grout. Furthermore, concepts used for minimizing possible defects during execution and for monitoring and minimization will also be considered.

2.5.3 State of Work

The achievable quality of grouted joints casted under offshore conditions is of great importance regarding both, function and lifetime of the structure as well as the turbine. Deep knowledge of the grouted joint quality is also important for the optimization of these types of connections. Currently, the once finished grouted joint is like a black box [3]. A quality evaluation seems up to now nearly impossible. Nevertheless, it is already possible to control the quality of the fresh and hardened grout outside the grouted joint.
An estimation of the grouted joints quality can be provided by a sensitivity analyses. For these analyses, hotspots within the construction providing a high possible risk of failure need to be found. The next step is to evaluate these risk factors which are dependent on the supporting structure and the place where the OWT is planned.
Each sensitivity analyses highly relies on variables which influence the quality of the grouted joint.
It is possible to separate these variables into four main groups. These are the grout-material, the application method, the design of the construction, and the offshore conditions.

Material

Relevant grout properties are the fresh, the hardening, and the hardened properties. Furthermore, the materials robustness is important for offshore applications.

Figure 1: Segregated grout

The most relevant fresh grout properties are the flowability, pumpability, viscosity, stiffening behaviour and the stability against segregations [5]. An example for a segregated grout is shown in figure 1.

Shrinkage [5] and the grout behaviour under early age cycling [1] are important hardening properties.
Compressive strength as well as its fatigue behaviour are relevant properties of the hardened grout. Moreover, the influence of different water to solid values and the behaviour under different temperatures [3] are important for robustness. Further to be considered is the storing stability of the dry grout material and the homogeneities between different batches.

Application Method

The mixing unit and the pump are also variables for the quality [6]. Different types of pumps and mixers might influence the grout properties; e.g. temperature, flowability and homogeneity of the material. Furthermore, an impact on the compressive strength is possible. For the application process the material of the pump line, the length of the line and the diameter have to be taken into account [2]. Moreover, the duration of the grouting process could have an influence on the grout homogeneity.

Type of construction

Influencing factors from the construction of the OWT and the grouted joint are the width of the gap between the pile and the sleeve as well as shear key geometry and the rate of the shear keys are also influencing variables. The length and possible imperfections of the connections are variables, too. Furthermore, the channel to distribute the fresh grout into the joint has to be considered. Main topics are the number and the size of the outlets and, whether the joint is filled with water or not.
Undesirable turbulences may lead to intermix of grout-material become if the grouted joint is filled with water as shown in figure 2. The behaviour of the grout is similar to figure 3 when no water is present.

Figure 2: Application process of grout into a grouted joint filled with water.

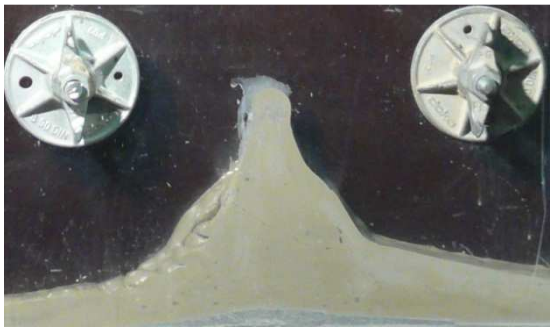

Figure 3: Application process of grout into a grouted joint without water.

Offshore Conditions

Offshore conditions do have a significant influence on the quality of grouted joints.
Harsh offshore conditions influence both, the material itself as well as the responsible staff on-site. Main factors are the ambient conditions like wind, waves and temperature of air and water [3].
The Offshore set up is another important influencing variable. Working procedures are different between a regular ship and a Jack-up Barge used as installation vessel. Figure 4 and 5 show these alternative types of installation vessels. “Jack-up Barges” are placed on the seabed after the jack up process. Such a barge is much more stable compared to a swimming installation vessel, but not as flexible and cheap as a ship. The responsible staff on site, facing harsh offshore working conditions is a key factor to the estimated offshore construction´s quality. Furthermore, the standards for health and safety are much more complex.

Figure 4: Jack-up Barge

Figure 5: Ship as an installation vessel

An example for proper protective clothing is given in figure 6.
To gain considerable experience, an institute´s research staff member received a special offshore safety and emergency training (basic offshore safety induction and emergency training, BOSIET). Two offshore operations in 2011 allowed the institute´s member to take a deeper look behind the scenes and to gain a valuable practical knowledge.

Figure 6: Immersion suit as work wear

References

[1] Welham , T.R..; Gilfrin, J.A: „Installation of Grouted Pile-Sleeve Connections: A-state-of-the-Art Review“. 25th Annual OTC, Houston, 1993.

[2] Domone, P.L.J.; Jefferis, S.A.: “Structural Grouts” Blackie Academic & Professional, Glasgow, 1994.

[3] Lohaus, L.; Lindschulte, N.: Offshore Windenergie Anlagen - Grouted Joints (Verarbeitung, Ausführung, Überwachung). Fachseminar ForWind, Bremerhaven, September 2011.

[4] Anders, S.; Lohaus, L.; Lindschulte, N.: „Oportunities and risks of steel fibres in Grouted Joints“. Proceedings, EWEC 2010, Warsaw, April 2010.

[5] Lindschulte, N.; Weicken, H.: „Hochleistungsmörtel und –betone in der Offshore-Windenergie“.
Heft 9 Berichte aus dem Institut für Baustoffe, Institut für Baustoffe, Leibniz Universität Hannover, Hanover, October 2011.

[6] Schmidt, M.; Braun, T: “Hochleistungs-Vergussbetone – Herstellung, Eigenschaften und Qualitätssicherung”. Seminar Grouted Joints bei Windkraftanlagen, Kassel, April 2011.

2.6 Monitoring of Mechanical Components (WP 6)

IMKT (Institute for Machine Elements, Engineering Design and Tribology)
Gerhard Poll, Janina Brencher, Roman Böttcher

In addition to the determination of safety elements for the civil engineering, safety- and reliability assessments of the mechanical and electronical components of the offshore wind turbines (OWT) will be considered.
The aim of work package 6 is the development and optimization of monitoring systems and diagnosis systems for bearings and screw connections. These systems should be applicable to OWT to provide reliable operation and efficient maintenance and should help to achieve basic knowledge during experimental studies on single components of the OWT drive train.

2.6.1 Motivation

The mechanical power train of wind energy systems is subjected to various non-stationary loads and speeds due to quickly changing operating conditions. These include sudden short time events like short circuits on the electric end and wind gusts on the rotor end. These external influences effect inter alia rapid accelerations in the drive train. The accelerations have particular effects, such as slip of rolling elements and subsequent smearing damages, on large size rolling bearings, as used in wind power plants, because of their higher mass-inertia compared to smaller bearings.
It is important to correctly be able to predict the effects of the influences on rolling bearings to predict the reliability and service life of mechanical components such as gears and bearings in order to avoid costly premature damage.
According to statistical analysis made by the German Wind Energy Institute (DEWI), different components of the wind turbine are causing different costs of maintenance, [1]. Figure 1 shows the statistical costs of maintenance of onshore wind turbines during an operation period of 20 years.

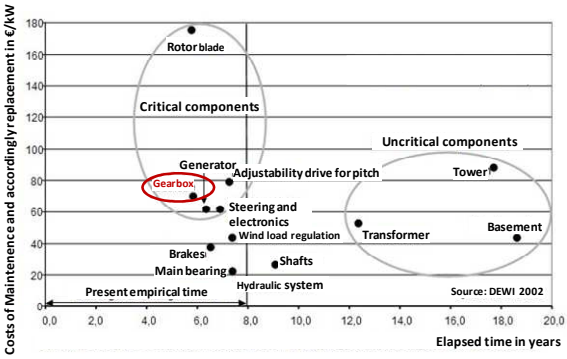

Figure 1: Costs of maintenance on wind turbines [1]

This figure clarifies that rotor blades, generator, adjustability drive for pitch, steering, electronics and the gearbox of a wind turbine are critical components for maintenance and replacement during early years of operation. All these critical components belong to the power train. The gearbox is a very important part of the power train, because it is positioned between the rotor blades and the generator. It changes low speed and high torque of the rotor blades to high speed and low torque for the generator. Figure 2 shows a configuration of a typical power train and its components in a wind turbine.

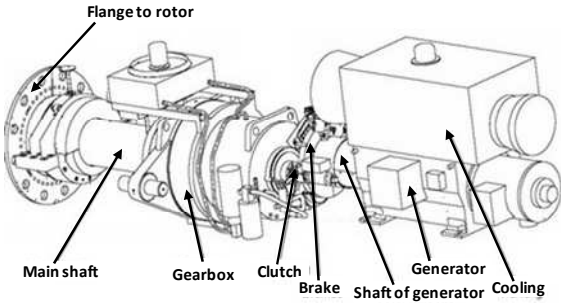

Figure 2: Power train of a wind turbine [1]

On the one hand, according to the characteristic of wind, the gearbox is loaded by changing speed and changing forces, on the other hand the characteristic of the generator influences the loads of all

components of the gearbox. A typical gearbox is designed with a ratio of transmission about 0.01. The gearbox consists of different sized gear wheels (including a planetary transmission), shafts and large size bearings. During the last years there have been some early failures on bearings mounted in gearboxes. Maintenance and accordingly changing of damaged bearings of the gearbox means high effort and costs especially for OWT.
The reliability of many mechanical components of wind turbines and possibly of OWT can be increased by control monitoring. This facilitates a better prediction of damages to bearings or gear wheels. In Addition to existing monitoring systems the aim of this project is the development and optimization of further suitable monitoring tools for early detection of damages. These tools should monitor damages of slow-rotating large size bearings and detect the preload of screw connections by integrated sensors.
If it is possible to measure the preload of important screw connections it might also be possible to measure forces that load bearings mounted in the gearbox.

2.6.2 Approach

For the monitoring of damages on dynamic slow-rotating large size bearings, existing diagnosis systems have to be developed further. For testing large size bearings with dynamic speed and dynamic load a large size bearing test rig is at IMKT's disposal. This test rig is depicted in the figure 3.
It is intended for experimental investi-gations with large size bearings under various conditions, especially those that may cause unexpected bearing damages or failures in practical applications. The test rig accommodates one test bearing (red color in figure 3). This bearing can operate with different speeds, radial and axial forces as well as tilting moments and misalignments, both static and dynamic. The following picture shows an overall view of the test rig.

Figure 3: Large size bearing test rig at Institute for Machine Elements, Engineering Design and Tribology of Leibniz University Hannover

Fatigue life of small bearings with different loads and speeds can be tested at several small test rigs at IMKT.

Condition monitoring system

The fatigue life of rolling element bearings depending on the load history, which even includes singular events, is actually being studied at IMKT both experimentally and theoretically, see also [4]. This allows for more precise life prediction in the field. High shock loads and skidding between rollers and raceways, both circumferentially and axially are to be taken into account. The existing standardized life prediction methods are not sufficiently validated under such conditions and appear to be unable to explain a number of failures observed in practice. To complement the experimental and theoretical investigations, additional studies are planned to measure the operational conditions of bearings in the real application.
Condition monitoring plays a vital role in all the experimental work. Methods are being developed to detect failures reliably in a very early state. These will later on be applicable for the supervision of wind power plants in regular service.
Existing condition monitoring systems still have problems with early detection of beginning roller bearing damages of bearings mounted in gearboxes. This is basically caused by insufficient provision

for dynamic speeds of wind turbines. The following figure shows a typical damage at the outer ring raceway of a cylinder roller bearing.

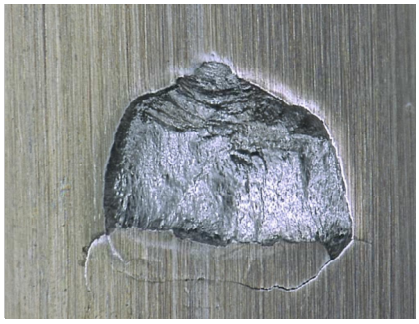

Figure 4: Pitting at outer ring of cylinder roller bearing

Present systems are successfully used for stations with constant speeds. High dynamic variability of speed demands special tools of evaluation and an exact consideration of the geometry of the gearbox. It is also a challenge to adapt a condition monitoring system to slow rotating large size bearings. [5]
The condition monitoring system developed during research at the IMKT was tested successfully at a four bearing test rig for smaller bearings, see also [6]. This system uses a FFT in combination with an envelope curve analysis for detection of roller bearing damages and therefore operates without the use of filter.
The vibration signal of bearing damages is recorded with piezoelectric accelerometers. The sensors have to be mounted in load direction and as close as possible to the specific bearing and its load zone. While the mounting of sensors could be taken in account during the development of new power plants, it is difficult to use the optimal sensor position on existing plants as well as on the large size bearing test rig described above.
The large size bearing test rig consists of a single test bearing and also two cylindrical roller bearings and one radially relieved four point bearing as support bearings, see figure 5. The axial and radial load on the test bearing can be applied by means of hydraulic cylinders both in tension as well as in compression.
Table 1 shows the number of possible sensor positions per bearing that would be necessary to perform a condition monitoring at every experimental combination of axial and radial loads.

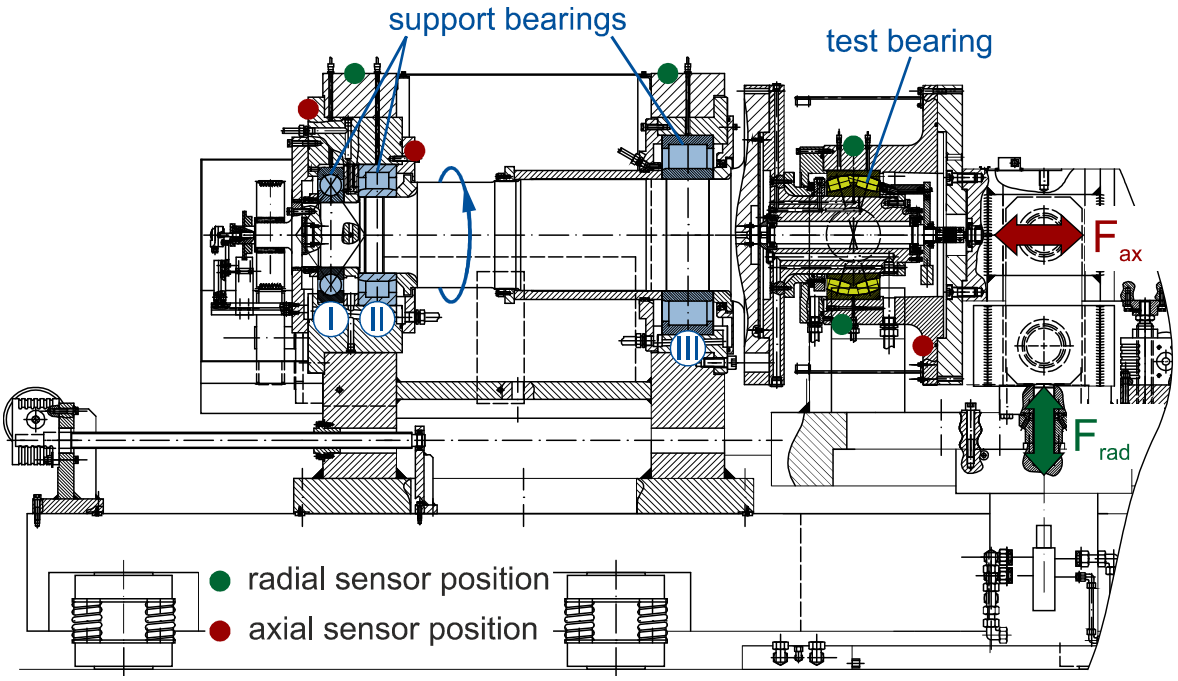

Figure 5: Actual sensor positions at the large size bearing test rig

Table 1: Sensor positions at the large size bearing test rig

Bearing	Number of sensor positions
Test bearing	2x axial, 2x radial
Support bearing I	2x axial
Support bearing II	2x radial
Support bearing III	2x radial
Total amount:	**10**

However, figure 5 shows the seven sensor positions that can be used at the moment on the test setup. Due to the lack of space, common acceleration sensors can't be mounted on the bottom of the support bearings in radial direction. An approach to the solution of this space problem could be in the use of thin film acceleration sensor elements. These thin film sensors are supposed to be tested on the large size bearing test rig under known conditions in direct comparison to common sensors on all positions, too.
The missing sensor in axial direction on the test bearing, see figure 5, will be installed after ending initial tests. This sensor has to be mounted inside the bearing housing, so that the sensor and the connection cable are exposed to the lubricant and high temperatures.

Preload of screw connections

The preload of screw connections can be monitored by special grommets or pressure blocks with integrated thin film sensors. The Fraunhofer Institute IST from Braunschweig has developed a system of grommets with special thin film piezoresistive sensors that are able to measure forces compressing the washer (see figure 6).

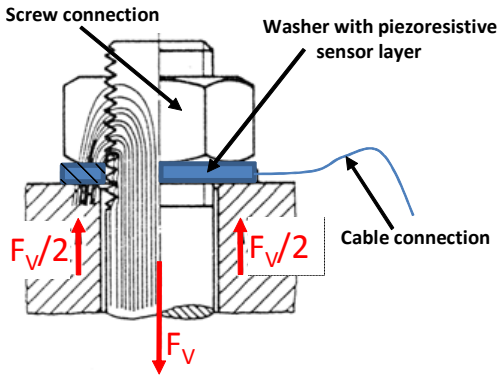

Figure 6: Screw connection with piezoresistive sensor [on the basis of 2]

The piezoresistive system consists of three thin film layers that are put on a substrate. Figure 7 shows the schematic configuration of these layers.

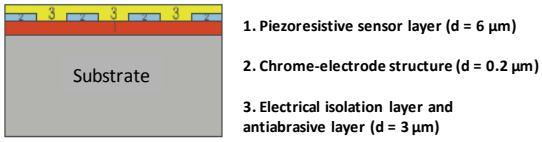

Figure 7: Schematic configuration of sensor layers [on the basis of 3]

It is possible to apply this system to different geometrical shapes and dimensions. In the future it might be possible to use RFID-chips for a wireless connection.
During the operation of mechanical components the forces acting on the screw connections can be recorded and the preloads of the mechanical components can be detected by using this new system of sensor washers. This makes it possible to permanently monitor the existence of the necessary preload of screws.
The aim of the project is to test and adjust the measuring method for use on OWT. Bearing test rigs are presenting a suitable possibility for purposive testing of this method under defined conditions. The testing and adjusting of this system to bearing test rigs will be done in two main steps:

1. Adjusting and testing the system in a load unit with springs mounted in

a test rig for small cylinder roller bearings (d_{shaft} = 30 mm). This allows using the system under defined constant load. In this way it is possible to evaluate long time behavior and temperature influence on the measurement.

2. Adjusting and testing the system on selected screws of the large size bearing test rig (d_{shaft} = 260 mm). The test rig enables testing under constant or dynamic conditions with higher forces that correspond to the forces of an OWT.

Step 1:

Figure 8 depicts the test head of IMKT's four cylinder roller bearing test rig. This test head is characterized by a constant load that is discharged radial into four equal test bearings with rotating inner ring or rotating bearing surface on the test shaft. The constant force is applied by a prestressed spring unit. It is possible to put a piezoresistive load sensor into the power train to measure and control the real forces during running the test bearings with constant radial forces.

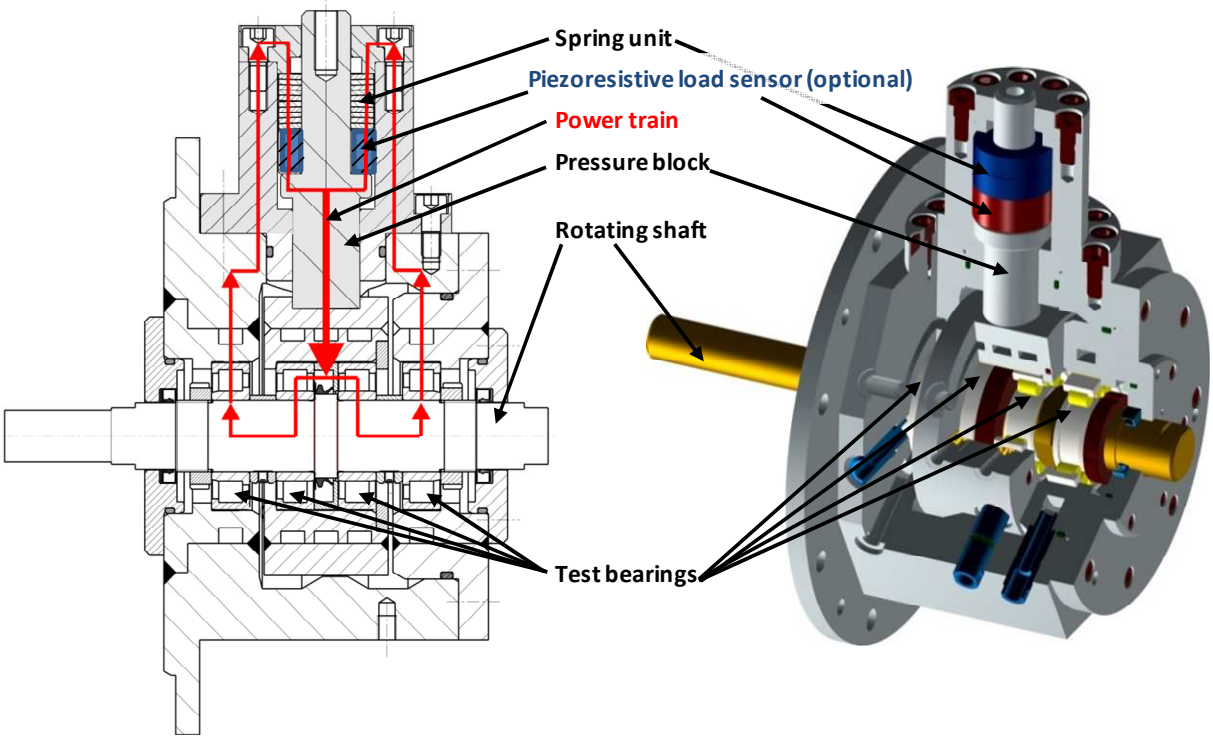

Figure 8: Test head of four cylinder roller bearing test rig (d_{shaft} = 30 mm).

Step 2:

The large size bearing test rig allows testing bearings that are normally mounted in gearboxes of wind turbines. It is possible to test these bearings under defined conditions. After having tested the piezoresistive load sensor system in a test rig for small bearings under constant conditions, the sensor system should be adjusted to conditions in the large size bearing test rig. The idea is to measure forces of chosen screw connections under defined dynamic conditions. By having notice of the forces of these screws it might be possible to calculate the real forces applied to the test bearing.

The test rig allows testing interference between forces of screw connections and forces applied to test bearing. Figure 9 shows an example of a screw connection on a bearing seat of a large size bearing at the test rig.

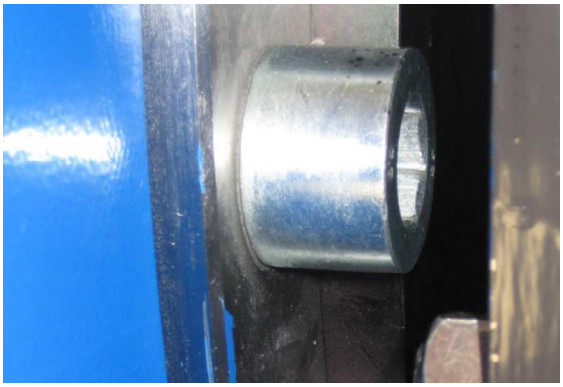

Figure 9: Screw connection on bearing seat at large size bearing test rig

If this method works it may also be possible to measure and record forces on bearings mounted in gearboxes of OWT. If these bearings are failing early it is possible to evaluate the correlation between the load history of the bearing and fatigue life. On the one hand this is very important with respect to the dynamic characteristics of the wind at low wind speeds and possible overloads and on the other hand with respect to the influence of the generator.

2.6.3 State of Work

Condition monitoring system

The described condition monitoring system is installed at the large size bearing test rig in an initial approach for adjustment and testing under defined conditions during run-ups and scheduled experimental investigations. Further implementation phases ensure the recording of vibrations signals on all sensor positions of the test bearing and a condition monitoring of the support bearings that aren't supposed to be replaced as often as the test bearings.
The condition monitoring system provides furthermore the early detection of bearing damages during fatigue tests on the four bearing test rig.

Preload of screw connections

The described system for measuring the preload of a prestressed spring unit in the four bearing test rig is just being manufactured. Next steps will be mounting, calibration and testing of this system under constant and defined conditions.

References

[1] DEWI 2002, study of the German Wind Energy Institute; www.wind-energie.de; 2010

[2] Steinhilper, Sauer; Konstruktions-elemente des Maschinenbaus Band 1; 7. Auflage; Springer; 2007

[3] On the basis of cooperation with Fraunhofer Institute IST; Braunschweig; 2010

[4] Hacke, Radnai, Hinkelmann; Berücksichtigung von Betriebszu-ständen, Sonderereignissen und Überlasten bei der Berechnung der Wälzlager-Lebensdauer in Windenergie-anlagen und Großgetrieben; Abschlussbericht FVA 541; Forschungs-vereinigung Antriebstechnik e. V.; 2010

[5] Hacke, B.; Reimers, E.; Hoffmann, G,: Neue Wege im Condition Monitoring, Antriebstechnik 12/2007.

[6] Hacke, B.; Früherkennung von Wälzlagerschäden in drehzahlvariablen Windgetrieben, Phd. Thesis, Verlag Dr. Hut, 2011

2.7 Diagnostic Systems for Electronic Systems (WP 7)

Institute of Drive Systems and Power Electronics
Meike Wehner

2.7.1 Motivation

Faults and defects in electrical machines, such as winding faults or rotor eccentricities, result in characteristical changes of the magnetic air-gap field, whose dependency on position and time was investigated in previous works at IAL-AS.
Using sensors such as search coils, the local dependence acts as a filter supporting the detection of a fault or defect with high signal to noise ratio as well as the identification of the type of fault by signal frequency.
In theory, the sensor signals are assumed to be zero in faultless wind generators. In industrial applications, the signal fluctuation as well as the reachable signal to noise ratio have to be evaluated. On the other hand, the influence of the generator type and the power electronic components concerning reliability have to be researched.

2.7.1 Approach

For this reason two diagnostic systems will be dimensioned and realized in prototypes. Finally, the measured data is evaluated, and based on this, appropriate design criteria are elaborated for this kind of diagnostic systems.

For the application in wind energy plants, three generator types are in common use. Besides doubly-fed induction machines and salient pole synchronous machines, permanent magnet synchronous machines have been used more and more during the last years. In a first step, a search coil system for 4-pole doubly-fed induction machines shall be dimensioned. The resulting air-gap field and the induced voltages in case of a fault are analyzed based on spatial harmonic theory by using the software ALFRED, which has been developed at IAL.

2.7.2 State of Work

Fault detection is made by tracking characteristic changes of the electromagnetic air-gap field. In [1,2,3,4], comprehensive investigations have been made concerning the appropriate arrangement of search coils. In [5], the layout of the search coil system for a doubly-fed induction generator with $2\mathrm{p} = 4$ poles and $\mathrm{N}_1 = 72$ stator slots is explained. The results of considerations are presented below.

The Layout of search coil systems can only be done optimally for a spatial harmonic with a certain number of pole pairs. As this reference number of pole pairs, $\nu_R = p - 1$ is selected, as it will be produced in all investigated failures (winding faults and rotor eccentricities), but not during normal operation of a symmetrical machine.
As a compromise between the number of conductors and the selectivity, a two-slot

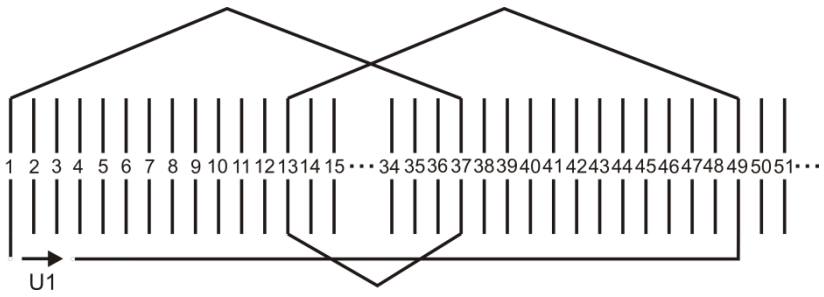

Figure 1: Winding distribution of search coil system in stator slots

winding is selected with the shift $\tau = 12$ respectively between the two coils. The pitch of each coil is $y_m = 36$. The distribution of the search coils in the stator slots is shown in figure 1

By using only one of these arrangements of search coils, the induced voltage in the search coils depends on the arbitrary angular displacement between fault location and coil system. In order to avoid this local dependence, a second identical search coil system is used, shifted towards the first one along the circumference by slots by 9 slots (half a pole pitch of the reference spatial harmonic).
This 2-phase search coil system allows to calculate the symmetrical components of the induced voltage and thus to detect the direction of rotating of the inducing spatial harmonic. The positive sequence component U_m is induced in case the reference spatial harmonic has the same direction of rotation as the rotor, the negative sequence component U_g is induced in case of reverse rotating direction. A zero sequence voltage doesn't exist in two-phase-systems.
Table 1 explains how the type of fault can be recognized from frequency and symmetrical component of the induced voltage.

For several faults, analysis is done by using the software ALFRED, which was developed at IAL. The software determines in accordance with the mathematical derivations in [3] and based on the spatial harmonic theory the resulting air-gap field as well as the voltages induced in the search coil system.

Eccentricities

Eccentricities which are not detected in sufficient time may provoke a rubbing of the rotor against the stator bore, shortly resulting in a complete failure of the machine.
In electrical machines, two kinds of eccentricities can appear. In case of a static eccentricity, the position of the smallest air gap remains at the same spot on the circumference, as shown in figure 2. In case of a dynamic eccentricity, the position of the air gap rotates with angular velocity of the rotor (figure 3).
Static eccentricities are described by the relative static eccentricity ϵ_{sta}, and the angle φ_{sta}. ϵ_{sta} describes the shift of the rotary axis of the rotor from the bore center related to the geometrical air-gap length. φ_{sta} indicates the direction, in which the rotary axis is shifted at static eccentricity,

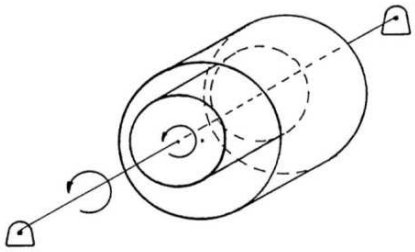

Figure 2: Static eccentricity

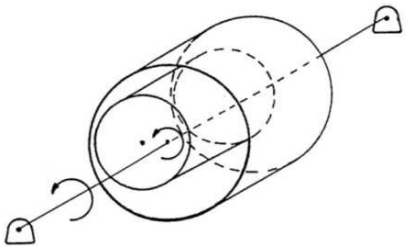

Figure 3: Dynamic eccentricity

Table 1: Fault Indicator [2]

Fault type	**Measured variable** f	**Symmetrical components** $U_m; U_g$
Winding fault	$f = f_1$	$U_m \neq 0; U_g \neq 0$
Static eccentricity	$f = f_1$	$U_m \neq 0; U_g = 0$
Dynamic eccentricity	$f = f_1\left\{1 \pm \left(\frac{1}{p}\right)(1-s)\right\}$	

i.e. the angle between the smallest spot in the air gap and the origin of the stator coordinate system.

The frequency analysis of the voltage induced for a static eccentricity of 30% of the air-gap width leads to frequency components with uneven multiples of line frequency, the amplitude being largest at line frequency (figure 4). For the relevant line frequency, the separation of the induced voltage in its symmetrical components shows a purely positive-sequence component. It is thus a good indicator for a static eccentricity.

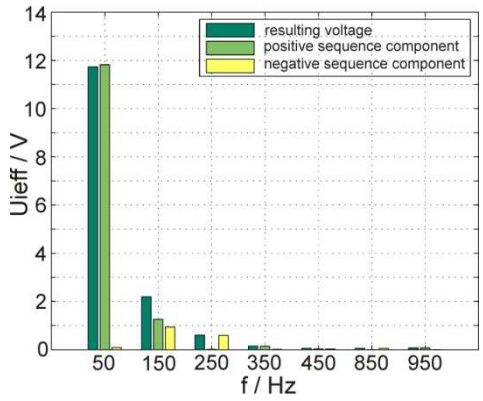

Figure 4: Frequency analysis of the voltage induced for a static eccentricity of ϵ_{sta} = 30 %

Figure 5 shows the voltages induced in the search coils for static eccentricities of 10% to 40% of the air-gap width. The amplitude of the voltage increases proportionally to the eccentricity and is thus a measure for the amount of eccentricity.

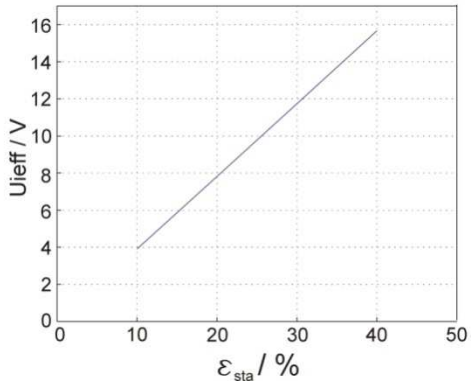

Figure 5: Induced Voltage at line frequency for different static eccentricities

By using a 2-phase search coil arrangement, the voltage induced is independent of the fault location.

Equivalently to static eccentricities, dynamic eccentricities are described by the relative dynamic eccentricity ϵ_{dyn} and the angle φ_{dyn}. ϵ_{dyn} indicates the shift of the rotor center from its rotary axis related to the geometrical air-gap length. φ_{dyn} indicates the direction, in which the rotor center is shifted in case of dynamic eccentricity. Figure 6 shows the frequency spectrum of the voltage induced in the search coils at dynamic eccentricity. According to table 1, for dynamic eccentricity and the selected reference number of pole pairs

$$\nu_R = p - 1 \tag{1}$$

voltages of the frequency

$$\mathrm{f} = f_1 \{1 - \frac{1}{p}(1 - s)\} \tag{2}$$

are induced in the search coil system. Based on the component with 25 Hz at $s \approx 0$ which is dominating in the voltage spectrum, a dynamic eccentricity can be clearly detected.

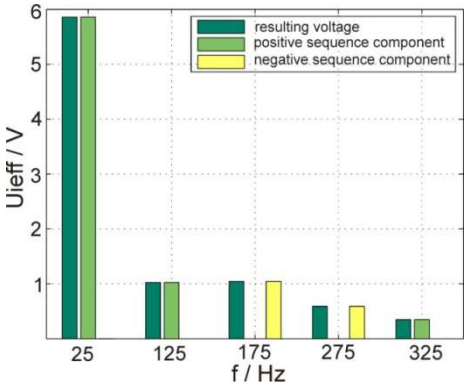

Figure 6: Frequency analysis of the voltage induced for a dynamic eccentricity of ϵ_{dyn} = 30 %

The voltage induced increases proportionally to the dynamic eccentricity, so that here too, clear conclusions can be drawn about the degree of eccentricity (figure 7). As for static eccentricities, the

search coil system implies no dependency on the fault location.

Signal to noise ratio

In theory, no voltage is induced in the search coil system of a faultless generator. In practice however, also in faultless mode small eccentricities, e.g. due to shaft bending or inaccuracies during assembly,

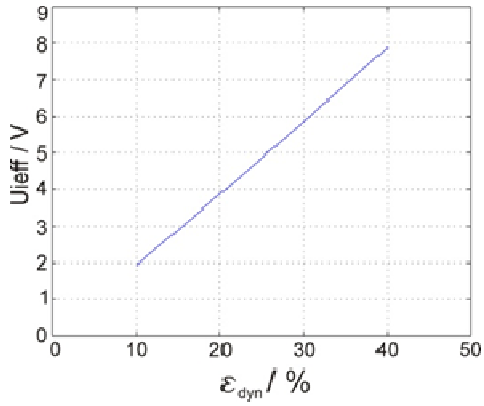

Figure 7: Induced Voltage for different dynamic eccentricities at a frequency of 25 Hz

cannot be completely avoided. So voltages are induced in the search coils. For this reason, it is investigated by means of interturn faults, in how far existing residual eccentricities have an effect on the fault detection and how large is the signal to noise ratio in this special case. The signal to noise ratio defines the ratio of the sensor signal, when the fault occurs, to the value in faultless mode.

First, the effect of an existing static eccentricity on the voltage induced in the search coils in case of an occurring interturn fault was examined. The short-circuit current assumed is 1000 A at line frequency. The residual static eccentricity was assumed with $\epsilon_{\mathrm{sta}} = 20\,\%$ and fault location $\varphi_{sta} = 30\,°$.

As indicator for the interturn fault, the line-frequency component of the voltage induced is considered. Figure 8, 9, and 10 show the characteristics of the voltage induced for different locations of the search coils along the circumference and different fault locations of the interturn fault for the line frequent component of the voltage induced in one of the two search coil phases only as well as for the symmetrical components.

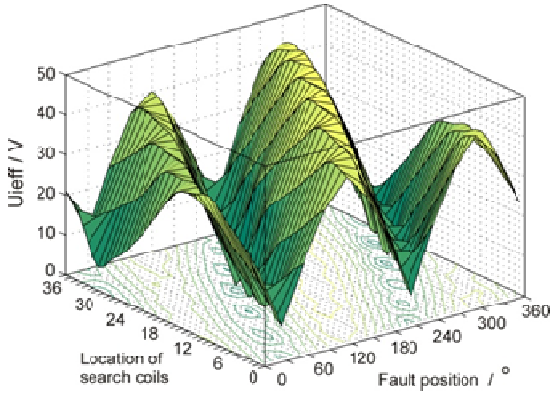

Figure 8: Induced resulting voltage for an interturn fault with static eccentricity of ϵ_{sta} = 20 % and φ_{sta} = 30 °

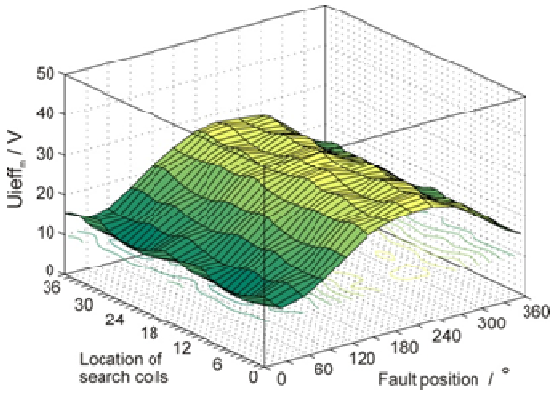

Figure 9: Positive sequence component of induced voltage for an interturn fault with static eccentricity of ϵ_{sta} = 20 % and φ_{sta} = 30 °

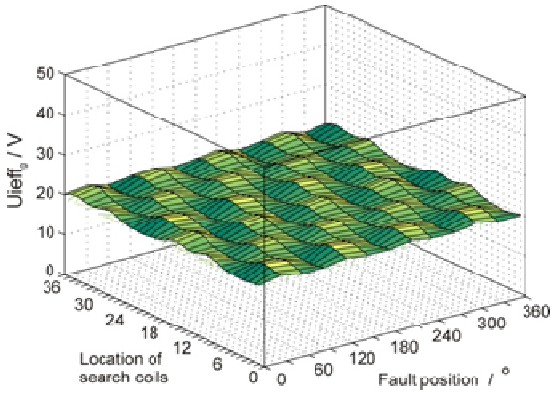

Figure 10: Negative sequence component of induced voltage for an interturn fault with static eccentricity of ϵ_{sta} = 20 % and φ_{sta} = 30 °

In order to determine the signal to noise ratio SN the voltage induced at interturn fault with static eccentricity U_{ieff} are compared to the voltage induced $U_{ieff,sta}$ at residual static eccentricity only.

$$SN = \frac{U_{ieff}}{U_{ieff,sta}} \quad (3)$$

The voltage in one of the two search coil phases only strongly depends on the fault location and is not suitable for a reliable failure diagnosis. Also the positive sequence component is more or less dependent on the position. As can be seen in figure 11, the signal to noise ratio varies correspondingly. Figure 12 shows the negative-sequence component of the voltage induced. The interturn fault can be clearly identified based on this voltage component, independent from the static eccentricity.

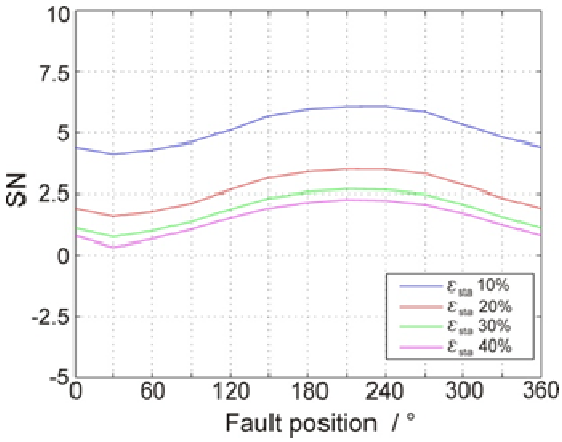

Figure 11: Signal to noise ratio of positive sequence component for different static eccentricities

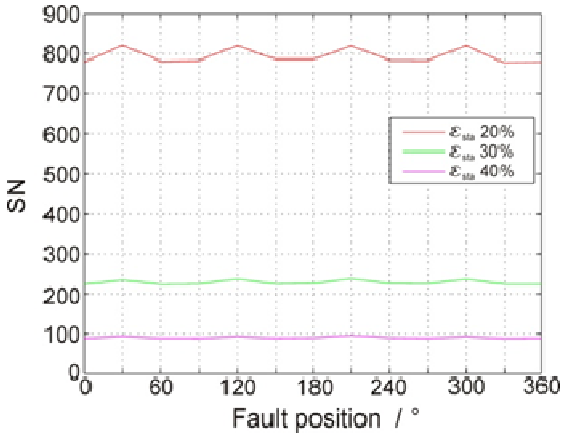

Figure 12: Signal to noise ratio of negative sequence component different static eccentricities

Conclusion

Using the search coil system dimensioned before, static and dynamic eccentricities can be identified for the simulated wind generator, based on the frequency components of the induced voltage which are characteristic for the type of fault. The amplitude of the voltages induced here is a measure for the amount of eccentricity. In addition, it was determined, in how far the detection of an interturn fault will be influenced by an existing static eccentricity, which for example can be caused by a misalignment during the assembly of the generator. Independent of the amount of eccentricity, the evaluation of the negative-sequence component is a good indicator for the detection of interturn faults.

References

[1] Pittius, E.; Analytische und Experimentelle Behandlung von Erdschlüssen in Asynchronmaschinen. Dissertation an der Universität Hannover, 1989. Fortschritt-Berichte VDI, Reihe 21, Nr. 48

[2] Früchtenicht, S.; Analytische und Experimentelle Behandlung von Wicklungsschlüssen in Asynchron-maschinen. Dissertation an der Universität Hannover, 1990. Fortschritt-Berichte VDI, Reihe 21, Nr. 56

[3] Ponick, B.; Fehlerdiagnose bei Synchronmaschinen. Dissertation an der Universität Hannover, 1994.

[4] Seinsch, O.; Rust, S.; Überwachung von Windungsschlüssen im Läufer von Induktionsmotoren mit Schleifringläufer, Elektrie, Berlin 50, 1996

[5] Wehner, M; Probabilistic Safety Assesment of Offshore Wind Turbines, WP 7, Annual Report 2010

2.8 Reliability of the Grid Connection (WP 8)

Institute for Drive Systems and Power Electronics
Felix Fuchs

Institute of Electric Power Systems
Stefan Brenner

Regarding the probabilistic safety of offshore wind turbines, the electrical system and the grid connection cannot be neglected. Together with work package 6 and 7, mechanical and electrical examination is covered.
The work package 8 is a collaboration between the Institute for Drive Systems and Power Electronics and the Institute of Electric Power Systems. The overall aim is to evaluate different grid connection topologies from the probabilistic point of view concerning the reliability. The two mentioned institutes are on the one hand specialized in the generator and its frequency converter and on the other hand in the grid connection itself.
The probabilistic reliability model of the whole electrical system will be implemented by the Institute of Power Systems, while the Institute for Drive Systems and Power Electronics delivers reliability models for power electronics and filter elements within the grid connection.

2.8.1 Motivation

In the field of electrical power supply the reliability of the system plays an important role. For the investor the breakdown of a wind turbine always means losses by reason of costs of repair and loss of (financial) compensation for electricity fed into the grid. Especially in the field of offshore wind parks a breakdown leads inevitably to long down times, because repairing takes longer due to limited accessability. In figure 1 it can be seen, that the higher the power of the wind turbines is, the more often the electrical part of the system fails. It is thus most important to investigate the reliability of the electrical system of large (offshore) wind turbines and their grid connection. The wind as a stochastic factor is an important input factor that determines load cycles and stress of the wind turbine. This gives also a motivation to examine the system from a probabilistic point of view.

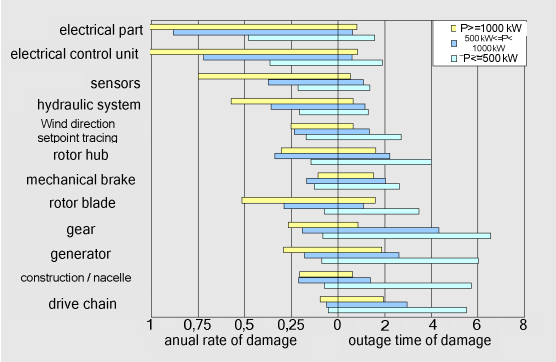

Figure 1: Frequency of damage and corresponding outage time of wind power plants sorted by components for different output power (from [1])

2.8.2 Approach

In figure 2, the topology of an offshore wind park, its internal interconnection and its connection to the onshore grid can be seen.

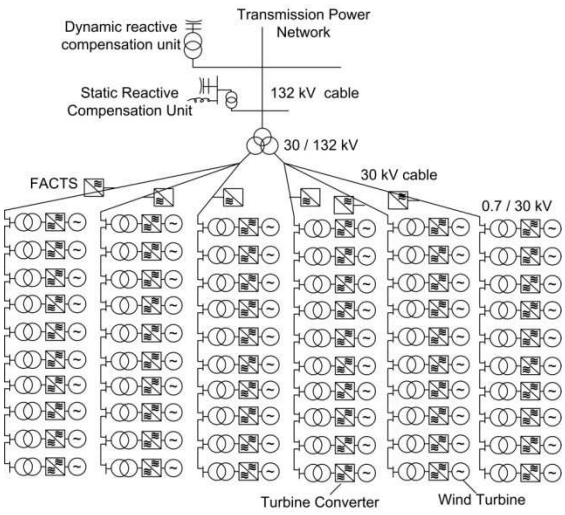

Figure 2: Example of the grid connection of an offshore wind park (in part from [2]).

Each wind turbine has a frequency converter, filters and a step up transformer. Other frequency converters

could control the power flow within the offshore grid (FACTS). Another step up transformer (30 kV /132 kV) gives the high voltage for transmitting the power through a sea cable to an onshore grid connection point. Compensation units (reactive compensation) help controlling the power flow. An alternative way to transmit the power onshore is a high voltage DC (HVDC) connection.

This overall system is in the focus of work package 8. All parts of the offshore grid concerning power electronics (frequency converters) and filters (capacitors, chokes) are covered by the Institute for Drive Systems and Power Electronics. Models giving information about their failure performance will be built. It is the aim to get a probabilistic model for the whole grid connection for computing the reliability. This will be done by the Institute of Electric Power Systems.

2.8.3 State of Work

From the side of the Institute for Drive Systems and Power Electronics, at first, the focus of the project lies on the frequency converter of an offshore wind turbine. In further steps, other frequency converters and filter elements will be considered. Weak elements of the power transmission chain in a wind turbine are the power semiconductor modules of the frequency converter [4]. So, the first aim is to get a probabilistic reliability model for the failure of the power semiconductors of the converter. In offshore wind turbines, mainly two topologies of generator-converter systems exist: The doubly-fed induction generator (DFIG) and the permanent magnet synchronous generator (PMSG). Both will be analyzed in this project.

Doubly-fed induction generator

The influence of operation statistics on the lifetime of power semiconductor modules in DFIG was investigated first. The most important factor influencing their lifetime is the varying junction temperature [4]. The junction temperature is dependent on the power flowing through the converter. With the software Matlab/Simulink/PLECS, it is possible to simulate the junction temperature variation of the power semiconductors.

A general sketch of the utilized procedure is shown in figure 3.

First, the junction temperature swings of the module (power semiconductors) over the wind velocity are computed in steady state operation. In the next step, the wind velocity data for 2009 (from the FINO station [3]) is taken. From this data, the operating time in 2009 for each wind velocity is calculated. The number of cycles with different temperature swing frequency and mean temperature is calculated. This is fed into a “cycles-to-failure-statistic” for the power semiconductor modules (taken from the LESIT project [5] or given by the manufacturer). For every wind velocity (discretized by 0,1m/s) the consumed percentual lifetime is computed. This is summed up linearly to a consumed lifetime in 2009.

A simulation model of the converter is extended with the thermal equivalent circuit of a standard low voltage module taken from its data sheet. A standard cooling system with the ambient temperature set to 40 degree is chosen. The equivalent thermal circuit of an IGBT (Insulate Gate Bipolar Transistor) module can be seen in figure 4.

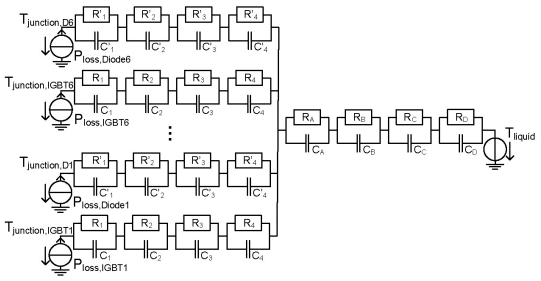

Figure 4: Thermal equivalent circuit of a power module with heat sink.

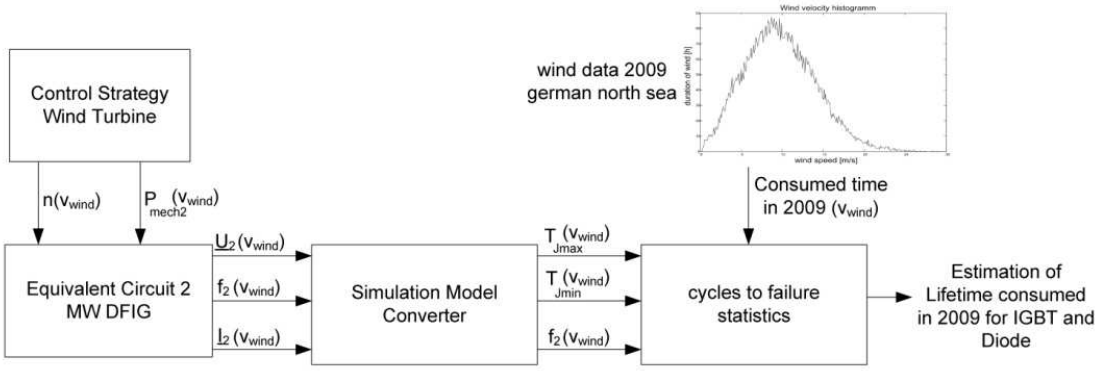

Figure 3: Procedure for lifetime estimation of the power module.

As input of this circuit, the absorption power P_v of the power semiconductors must be computed. It is composed of temperature dependent turn off, turn on and conducting losses specified by the data sheet.

A wind turbine model of a 2 MW DFIG is taken (for system parameters see table 1). The control system always tracks the maximum of the cp-characteristic of the wind turbine assumed (fixed pitch angle [2]).

Table 1: System Data.

Symbol	Quantity	Value
P	Rated Power	2 MW
U_L	Line voltage (phase-to-phase, rms)	690 V
ω	Grid frequency	2π50Hz
p	Pole Pairs	2
$f_{S,machine}$	Switching frequency machine side converter	3 kHz
n	Gearbox ratio	1:72,65
R	Turbine radius	37 m
v_{min}	Cut-in wind speed	3.5 m/s
v_{rated}	Rated wind speed	12 m/s

An example junction temperature swing of the machine side converter is shown in figure 5 for a wind velocity vwind=7.8 m/s.

It can be seen that in steady state the temperature oscillates with the frequency of the rotor current. The junction temperature of the IGBT and diode of one phase leg is taken and mean,
minimum and maximum values are extracted. For this analysis, two power modules were taken.

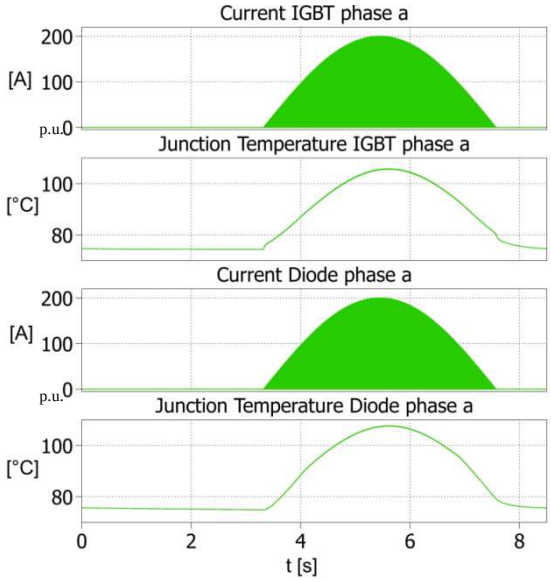

Figure 5: Currents and junction temperatures at steady state with v_{Wind}=7.8 m/s

One module is dimensioned to the simulated operating points and another is over dimensioned by a factor of two. Figure 6 shows the results for the low rated module (left column) and the high rated module (right column). It should be mentioned that for both systems
the same liquid cooling system with a temperature of 40 degree is chosen. The high rated module is not heating up as much as the low rated module. The tendencies are equal in both modules: with

increasing power the mean temperature of the modules increases until the rated operating point is reached where it has its maximum. With both modules, the temperature swing increases at the synchronous operating point. As expected in both modules - due to the fact that they include a standard diode - the diode has higher mean temperatures than the IGBT in the oversynchronous operating area.
The number of used temperature cycles in 2009 can be derived (assuming that the wind turbine only operates in steady state): The duration for a specific wind velocity has to be divided by
the electrical rotor period. In this way a rough lifetime estimation can be done, also revealing which operating point takes most of the lifetime. The results can be seen in figure 7 for the low rated module (left column) and the high rated module (right column). The consumed lifetime per 0.1m/s is plotted. In line with the results of the ZULES project [6] it can be stated, that the main lifetime consuming operation point is the rated wind velocity of 12 m/s. The synchronous operating point is not critical. Several cycles-to-failure statistics have been applied. The curve with the lowest lifetime, respectively the top trace in all plots corresponds to the LESIT results. The LESIT tests have been established in the end of the 1990ies. Until today the power cycling capability of modules was enhanced. So, for comparison, the cycles-to-failure statistics provided by the manufacturer are taken into consideration, too. The lowest curve is the one for the newest IGBT module, the one in the middle is for standard modules. The whole consumed lifetime can be seen in table 2. It can be said that the low rated module has a life expectancy of less than 0.25 years with an actual IGBT module.

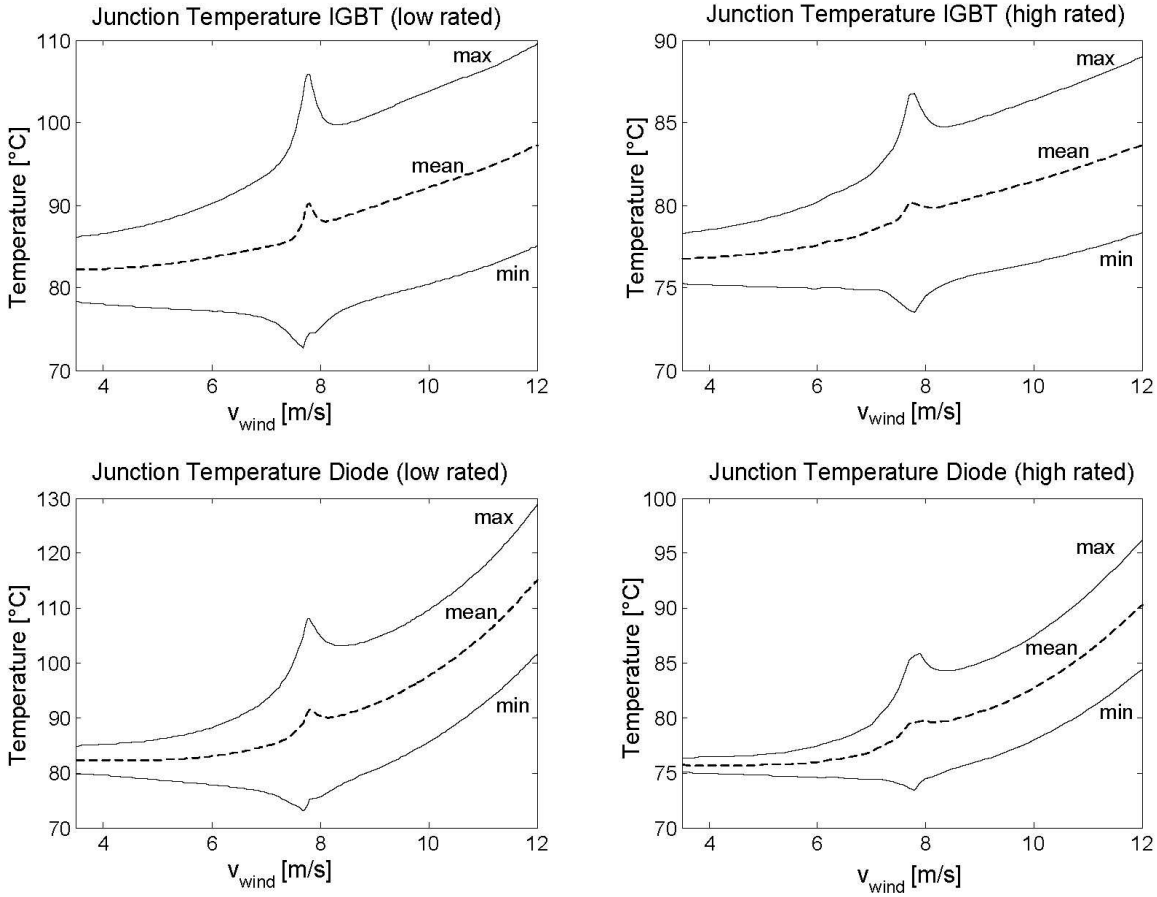

Figure 6: Junction temperature over wind velocity of IGBT (top) and diode (bottom) with low rated module (left) and high rated module (right)

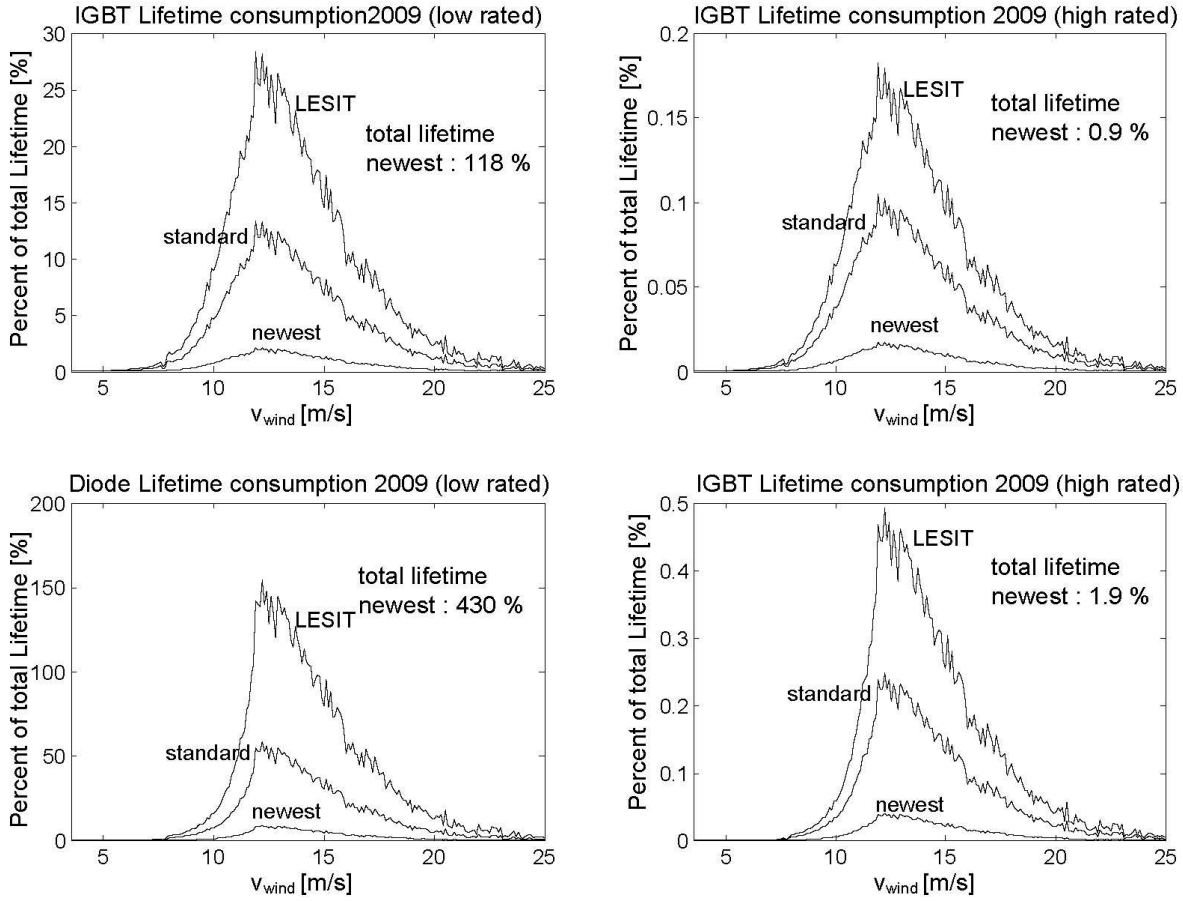

Figure 7: Lifetime consumption of IGBT (top) and diode (bottom) with low rated module (left) and high rated module (right) (different cycles to failure statistics)

This is not enough regarding the intentioned lifetime of 20 years. With the high rated (actual) module a very acceptable lifetime of approx. 50 years can be reached. It is interesting to note that the diodes are the limiting factor concerning expected lifetime.

In a next step, the work is focused on consideration of the dynamic operation of DFIG. Here, rain flow counting algorithms will be utilized to extract temperature swings caused by wind fluctuation [7]. Finally, a reliability model for the converter of the DFIG system will be built.

Permanent magnet synchronous generator

First experiences with the system of a permanent magnet synchronous generator were made, a simulation model including the generator side and grid side control was implemented. Here, a three-level NPC full power converter with medium voltage was chosen (figure 8).

A balancing algorithm for the DC-capacitors was included, too. The grid side control reacts on grid voltage drops according to the grid connection rules given by the transmission system operator. The results of the analysis of the DFIG are detailed in a publication [8].

Table 2: Consumed Lifetime for low rated and high rated module in 2009 in %

Cycles-to-failure statistic	IGBT, lr	Dio-de,lr	IGBT, hr	Dio-de,hr
LESIT	1542	7333	10	23
Industrial standard	736	2833	5.8	12
actual	118	430	0.9	1.9

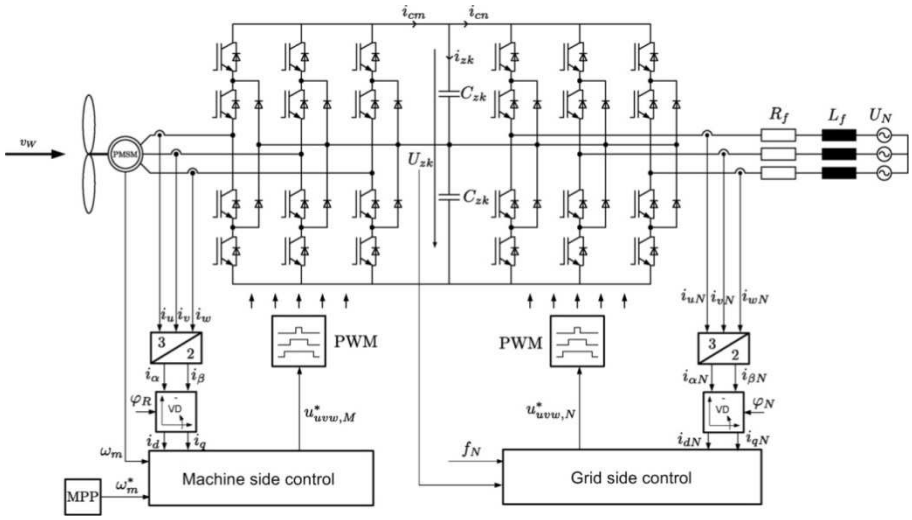

Figure 8: Schematic of PMSG wind turbine control system with three-level converter

The further steps of the project will be:

- Analysis of the dynamic operation of the DFIG
- Use the existing model to extract parameter sensitivities concerning also the stochastic wind velocities
- Extend the simulation model of the PMSG to power semiconductor lifetime analysis
- Analysis of the reliability of the DC capacitors in both systems

References

[1] ISET Kassel; Windenergiereport 2008 (in german).

[2] Lubosny, Z.: Wind turbine operation in electric power systems: advanced modeling and control, Springer, 2003

[3] Neumann, T.; Nolopp, K.: Erste Betriebserfahrungen mit der FINO1-Forschungsplattform in der Nordsee (in german), DEWI Magazin, 2004.

[4] Bartram M.; Bloh I.; Doncker R.; Doubly-fed-machines in wind turbine systems: Is this application limiting the lifetime of IGBT frequency converters; 35th Annual IEEE Power Electronics Specialists Conference Aachen, 2004.

[5] Held, M.; Jacob, P.; Nicoletti, G.; Scacco, P.; Poech, M.: Fast power cycling test for insulated gate bipolar transistor modules in traction application, Int. J Electron.,vol.86,pp. 1193-1204, 1999.

[6] M. Deicke and M. Schniedermeyer, “Zules: Thermal load of igbt-converters for wind turbines with doubly fed induction generator - final presentation,” BMBF-Verbundprojekt with SEG Woodwards, 2003 (in german).

[7] M. Sleven and J. Schiele, “Modern power module technology for wind turbine inverter with increased reliability,” VDE Kongress ’08 Munich (in german), Infineon Technologies AG, Max-Planck-Str. 5,D-59681, Warstein.

[8] Fuchs, F.; Mertens, A.: Steady State Lifetime Estimation of Power Semiconductors in Rotor Side Converter of a 2 MW DFIG Wind Turbine via Power Cycling Capability Analysis; EPE '11 14th European Conference on Power Electronics and Applications, 30 Aug.-1 Sept. 2011

3 Summary

Institute of Concrete Construction
Boso Schmidt, Michael Hansen

Within this project safety assessments of OWT structures and the grid-connection are carried out. Uncertainty is recognized by conventional deterministic design methods only implicitly and unequally. Thus, probabilistic methods are used to determine and consider statistical spreads within numerical analysis. Besides the support structure, the mechanical-electrical energy conversion and the electronic transformation up to the network supply are analyzed. The probabilistic methods as well as the common used measurement data reunite the project partners. Some results of contained work packages are briefly described below.

WP 1 describes basics of the current semi probabilistic safety concept. The question of a suited target reliability for OWT is treated, too. Finally, it is shown how to consider system reliability.

In the first part of WP 2 a failure mode and effect analysis of a generic OWT is prepared on basis of published information and with focus on the wind turbine system. The effects of site-specific wind field parameters are investigated by means of aeroelastic simulations, too. The second part deals with hydrodynamic questions. First of all analyses of the dominant and significant sea states in the North Sea on the basis of statistical analysis of extreme events are done. Afterwards, the wave-breaking probability is investigated by means of laboratory experiments in two- and three-dimensions.

In WP 3 it is shown that the estimated safety of laterally loaded piles is much higher as it would be reasonable for OWT. Additionally it is shown that the pile head moment has a significant influence on the safety and serviceability of an offshore foundation pile.

In WP 4 a numerical model of a monopile is implemented and validated. Based on a pool of data of FINO 1 measurement platform relevant values and statistical distributions of extreme action effects are determined.

WP 5 identifies probably relevant influences of the in-situ assembly on the material properties of grouted joints on site. Furthermore, laboratory tests were carried out to evaluate the effects of some of these probable influences on the grout material properties.

WP 6 shows that it is possible to detect fatigue damages on rolling element bearing with condition monitoring systems by means of classical vibration sensors during operation. For further advance, researches on alternative vibration sensor models as well as sensors for load monitoring are required. Thereby, existing wind turbines can be retrofitted and a basic understanding of fundamental failure mechanism of rolling fatigue in combination with the versatile operation conditions of OWT is gained.

In WP 7 using the search coil system dimensioned before, static and dynamic eccentricities can be identified for the simulated wind generator, based on the frequency components of the induced voltage which are characteristic for the type of fault. In addition, it was determined, how the detection of an interturn fault will be influenced by an existing static eccentricity, which for example can be caused by a misalignment during the assembly of the generator. Independent of the amount of eccentricity, the evaluation of the negative-sequence component is a good indicator for the detection of interturn faults.

WP 8 analyzes the Doubly Fed Induction Generator and the lifetime of the power modules of the rotor side converter. In addition, the other important generator system of wind turbines, the permanent magnet synchronous generator is examined with simulation models. Here, also the electrical behavior during grid faults is highlighted.

4 Literature

4.1 Publication List

4.1.1 Reviewed Articles

4.1.2 Reviewed Conference Contributions

Fuchs, F.:
Steady State Lifetime Estimation of Power Semiconductors in Rotor Side Converter of a 2 MW DFIG Wind Turbine via Power Cycling Capability Analysis.
EPE'11 ECCE 4th European Conference on Power Electronics and Applications, Birmingham (UK), 30.8. – 1.9.2011

Neubauer, T.:
Quantifizierung von Leistungsdichtegrenzen von Wälzlagern zur Vermeidung von Drehzahlschäden.
Informationstagung 2011 der Forschungsvereinigung Antriebstechnik e. V., 23.-24.11.2011, Würzburg, FVA Forschungsreport 2011

Poll, G.:
Fluid Rheology, Traction/Creep Relationships and Friction in Machine Elements with Rolling Contacts.,
38. Leeds-Lyon Symposium on Tribology, 6.-9.9.2011 Lyon (Fr)

Poll, G.:
Rheologie von Schmierstoffen in konzentrierten Wälzkontakten.
7. Arnold-Tross-Kolloquium, 17.06.2011, Hamburg

Schmoor, K.; Achmus, M.:
On the influence of the variability of soil parameters on the behaviour of laterally loaded piles in sand.
Proceedings of the 9th International Probabilistic Workshop, 17.11. – 18.11.2011, Braunschweig

4.2 Doctoral, Diploma, Master and Bachelor Theses

Diekmann, H.; Meister, S.:
Auswirkungen von Wassergehaltsschwankungen auf die Frisch- und Festmörteleigenschaften von Vergussmörteln für Grouted Joints.
Study Thesis
IFB May 2011

Ebrahimi, M.:
Investigation of the Thermal Load of Power Semiconductors Used in Wind Turbines with Doubly Fed Induction Generator.
Master Thesis
IAL February 2011

Gossmann, A.:
Konstruktive Anpassung und Erweiterung eines Prüfstandskonzeptes für Wälzlager eines Windkraftanlagenbetriebes.
Project Thesis
IMKT January 2011

Hacke, B.:
Früherkennung von Wälzlagerschäden in drehzahlvariablen Windgetrieben.
Doctoral Thesis
IMKT February 2011

Koch, M.:
Analyse von Netzfehlern bei Windenergieanlagen mit permanenterregter Synchronmaschine und Mittelspannungsumrichter in der Simulation.
Master Thesis
IAL March 2011

Schultenkämper, M.:
Probabilistische Voruntersuchung einer Gründungskonstruktion für Offshore-Windenergieanlagen.
Study Thesis
IFMA June 2011

Smirnov, A.:
Simulation eines rauen Wälzkontaktes unter Berücksichtigung von Reibung.
Diploma Thesis
IMKT October 2011

Wendland, J.:
Modellversuche zur Analyse baustofflicher und herstellungsbedingter Einflüsse auf Grouted Joints.
Diploma Thesis
IFB September 2011